Concept of a One-Moment Ice Cloud Scheme Avoiding Saturation Adjustment

-

Konzept eines Ein-Momenten Eiswolken Schemas ohne Sättigungskorrektur

Master's Thesis at the Faculty of Physics
of the
Ludwig-Maximilians-Universität München

submitted by

Dario Sperber

born in Münster

München, 21.07.2023

Abstract

Persistent contrails and contrail induced cirrus are responsible for a large fraction of global aviation's effective radiative forcing. The persistence of contrails could be avoided by rerouteing aircraft around ice supersaturated regions in the upper troposphere. Unfortunately, the forecasting of these regions is challenging, where one of the problems are inaccurate ice cloud parameterisations in numerical weather prediction models, many of them making use of "saturation adjustment". In this approximation, the air inside ice clouds is assumed to be exactly saturated, even though supersaturated water vapour is frequently observed inside cirrus.

In this thesis, the concept of a new one-moment ice cloud scheme avoiding the use of saturation adjustment is proposed. A simple humidity distribution for newly generated cloud parts is derived with the help of a stochastic box model that treats one model grid box as an ensemble of a large number of individual air parcels. This distribution is used to model the decay of in-cloud supersaturation explicitly in two alternative parameterisations. One introduces the in-cloud humidity as an additional prognostic variable in order to evolve it in time. The other one adjusts the in-cloud humidity to its equilibrium value in some cases, but in turn does not need an additional prognostic variable.

The new parameterisations are then tested against a parameterisation that uses saturation adjustment, where the stochastic box model serves as a benchmark. It is shown that saturation adjustment underestimates humidity both shortly after nucleation, when the actual cloud is still highly supersaturated, and also in aged cirrus if cooling proceeds, as the actual cloud remains in a slightly supersaturated state in this case. In contrast, the new parameterisations show great improvement compared to saturation adjustment, as they stay closer to the stochastic box model in any considered case. It is concluded that the new parameterisations are promising, but need further testing in more realistic frameworks.

Contents

Chapter 1

Introduction

The dream of flying used to be one of the most desperate desires of mankind since ancient times. Countless great minds dedicated their lives to inventing a machine that would lift human feet off the ground and up into the skies. Nevertheless, it still took thousands of years from antique myths like Daedalus and Icarus (33) over the first promising ideas of Leonardo da Vinci (e.g. 4) until the dream finally came true, when pioneers like Otto Lilienthal and the Wright brothers performed their first flights. Nowadays, civil aviation can fulfil this ancient dream for basically anyone. More than 100 years of science and industry long have overcome issues like safety or distance limitations. It is a different problem that forces people into the streets demonstrating against modern air transportation and that science will have to solve in order to keep the dream alive for future generations: Climate Change.

1.1 Aviation's Climate Impact

Civil aviation in its current form is not at all conformable with mitigation goals like "climate neutrality", since it is already responsible for about 3.5% of the total anthropogenic effective radiative forcing (ERF) and future projections show a steep, further increase in passenger kilometres of about 3.6% per year (42). Decarbonisation of the aviation sector will take several more decades and even achieving carbon-neutral air transportation would not reset the ERF to zero, as the amount of CO_2 already emitted into the atmosphere will affect climate for hundreds of years. Furthermore, the climate effect of air traffic is not only caused by the fossil CO_2 emissions, which may be avoided by running hydrogen or synthetic kerosene powered aircraft. Recent results suggest that more than half of aviation's ERF is generated by so-called non-CO_2 effects and many of these cannot be mitigated by a change in aircraft fuel. Among these non-CO_2 effects, the largest ERF components are caused by persistent contrails and contrail induced cirrus, the emission of nitrogen oxides and the injection of water vapour into the stratosphere, where the contrails dominate over the other two effects in terms of radiative forcing and effective radiative forcing. However, unlike the CO_2 emissions, contrails are radiatively active for at most several hours and do not remain in the atmosphere for hundreds of years. Consequently, a hypothetical mitigation of the further generation of all persistent

contrails would not only stop the further increase of this component of aviation's ERF, it would actually drive it down to zero quickly, once all persistent contrails had disappeared. Therefore, avoiding these contrails can be considered an effective measure in slowing down the further increase in the overall anthropogenic ERF as quickly as possible which is crucial in order to lower the peak of global warming that we have to expect. Decarbonisation can only assure a long term decrease of aviation's ERF. (25)

However, the climatological mean ERF of persistent contrails is, even though significant, still quite uncertain. This is not surprising given the fact that even estimating the radiative impact of single contrails is challenging due to three difficulties in modelling their lifecycle which also render their mitigation a serious challenge: First, the impact of each individual contrail is highly sensitive to the surrounding synoptic situation and can range from strongly cooling to strongly warming (50). Thus, it is not meaningful to avoid all persistent contrails and one has to estimate in advance, where the avoidance is worth the effort. Second, one of the most important parameters in the synoptic environment of the contrail is the relative humidity, which is highly variable in space and time, but is still lacking a sufficient amount of proper measurements on cruise levels. As a result, the synoptic environment of the contrail cannot be characterised with a precision that would be necessary for an accurate simulation of its lifecycle and thus its immediate radiative effect. Finally, even if the synoptic environment was properly measured, the parameterisations for cirrus clouds in current numerical weather prediction (NWP) models mostly make use of rough approximations to reality. This leads to a systematic underestimation of the occurrence frequency and degree of ice supersaturation in the upper troposphere in the performed simulations (10), which again impedes the proper evaluation of a contrail's immediate radiative effect.

1.2 Ice Supersaturation and its Generation

Nevertheless, even though its magnitude is uncertain, persistent contrails are responsible for a significant ERF and it thus is an important step on the way to more sustainable air transportation to mitigate this radiative impact. But in order to avoid them, one first has to understand how these contrails are formed (Schmidt-Appleman criterion, see 38, 1, 39) and when they persist. An important condition for their persistence is ice supersaturation which is a quite uncommon phenomenon in everyday life but quite common in the upper troposphere. The following explanations are based on Lamb and Verlinde (24), where further details are available in chapters 7 and 8.

Whenever a surface of condensed water, i.e. ice or liquid water, is present, water molecules from the gas phase continuously transfer into the condensed phase and high energy molecules from the condensed phase transfer in the opposite direction. If the water surface is plain and free of pollutants, the relative humidity in the air above the surface is defined as 100% and the air is referred to as saturated, whenever these two transition rates are equal. Since the water molecules in an ice surface are bound stronger than in a liquid surface, they require more energy to leave the condensed phase and thus can do so less often. Therefore, at a given

temperature, the escape rate from the condensed phase is lower in the case of an ice surface and thus an equilibrium of the two transition rates is reached at a lower specific humidity of the air. Hence, 100% relative humidity with respect to ice correspond to a lower specific humidity than 100% with respect to liquid water at the same temperature. If the respective relative humidity rises beyond saturation, the air is referred to as supersaturated with respect to ice or liquid water.

However, in the atmosphere, large supersaturations with respect to liquid water are uncommon, since air always contains aerosol. A large fraction of these particles serves as condensation nuclei, where water vapour condenses on already at slight supersaturations (often a fraction of a percent), forming droplets that consume the supersaturation. For ice this is different. Ice features a crystalline structure which is generally something very unlikely to form by chance. Thus, solid aerosol particles that support ice nucleation have to offer structures with similar lattice parameters on their surfaces. Since such particles are very rare in the upper troposphere, this way of ice formation, termed heterogeneous nucleation, is commonly not the dominant nucleation process (14). Instead, ice in the upper troposphere rather forms via homogeneous nucleation, i.e. via the freezing of liquid aerosol particles. These far more abundant particles are microscopic droplets of aqueous acid solutions which remain liquid even at temperatures below -38°C which is the approximate limit for the supercooling of pure water droplets. The reason is the presence of the large acid molecules that inhibits the organisation of the water molecules into a crystalline lattice. Therefore, homogeneous freezing is only possible if the solution becomes sufficiently dilute which requires large supersaturations with respect to ice in the ambient air of more than 40%. As a result, upper tropospheric air is frequently found in a state of significant ice supersaturation, both in clear air before nucleation occurs (e.g. 11, 34) and within cirrus clouds (32, 44, 3).

1.3 Contrails and their Mitigation

If now an aircraft flies through the upper troposphere, its engines emit large amounts of both, water vapour and aerosols, mostly soot polluted by other materials (see 16, for an overview). Whenever the Schmidt-Appleman criterion is fulfilled, the mixture of this exhaust with the environmental air is going to exceed water saturation such that the vapour will condense on the aerosol particles creating small but fast growing droplets, i.e. a contrail is formed. In the course of further mixing with the environmental air, this young contrail will approach the environmental temperature. If this temperature is below about -38°C the contrail will freeze, usually homogeneously, depending on the nature of the individual condensation nuclei. Finally, it then is the background relative humidity that decides, whether these ice crystals are going to sublimate again in the case of background ice subsaturation or whether they are going to grow further in size by deposition forming a persistent contrail in the case of background ice supersaturation.

If a contrail has formed, no matter its lifetime, it scatters solar light back to space, but also absorbs infrared radiation from Earth's surface and lower atmospheric levels, and thereby

traps the energy inside the Earth system (e.g. 30, 2, 41, 52), just like natural cirrus clouds. Thus, contrails have both warming and cooling effects on the Earth system, but on average the warming dominates. However, the net radiative effect of a single contrail depends on multiple parameters such as the time of day or the albedo of Earth's surface underneath and it can be warming as well as cooling. The distribution of instantaneous radiative effects is wide (50), and so is the distribution of contrail lifetimes (13) such that one can imagine that the overall radiative effect of single contrails (energy forcing, see 41) varies widely as well. Fortunately, this means that the contrail share to the climate effect of aviation can already be reduced drastically by only avoiding those contrails that exert the strongest warming impact (46, 45). These contrails are also the ones, whose sign of impact (warming or cooling) should be predictable with the highest certainty such that one can focus on mitigating these contrails and ignore the ones where the uncertainty whether they are cooling or warming is high.

In order to do so, flight routes need to be planned or adjusted in a way that regions, where strongly warming contrails are expected to form, are avoided. To achieve this, it takes three steps: First, predict, where contrails may form (i.e. where the Schmidt-Appleman criterion will be fulfilled, see 39); Second, predict, where they would persist (ice supersaturated regions, see 12); and third determine or estimate their individual radiative effect either by simulating their development (40) or, if a forecast is needed quickly, by using so-called algorithmic climate change functions (aCCFs, see 53, 5). This information can then be used to determine, whether the radiative effect of an individual flight can be reduced by rerouteing the aircraft around an ice supersaturated region or whether this would enlarge the radiative effect due to the associated increase in fuel consumption. Sausen et al. (37) could show that such contrail avoidance is possible in operational air traffic management, but step number two currently represents the bottleneck to a more successful avoidance, since the prediction of ice supersaturation is, as mentioned earlier, quite challenging.

On the one hand, this is due to the nature of the upper tropospheric humidity field. Satellite imagery taken in the water vapour absorption band at about 6 to 7 μm shows that it is highly variable and commonly features sharp gradients. Water vapour participates in dynamic, thermodynamic, chemical and aerosol processes on a multitude of spatial and time scales. Furthermore, the critical variable for ice supersaturation is the relative humidity, which does not only depend on the absolute humidity but also on temperature. As a consequence, the upper tropospheric relative humidity features huge variability and these circumstances alone already make the prediction of this field quite difficult. But ice supersaturation is an extremal state of the humidity field which is more sensitive to changes of external conditions than bulk measures of humidity, for example if nucleation thresholds are exceeded. Clearly, a field that variable would need a dense measurement network in order to be predicted with a precision in time and space sufficient for sustainable flight routeing. Unfortunately, data assimilation in NWP is currently lacking reliable humidity measurements on cruise levels, where an effective solution could be equipping more commercial aircraft with reliable humidity sensors.

On the other hand, modern NWP models still would not be able to provide reliable forecasts of ice supersaturation in the upper troposphere even if the relative humidity field was

properly measured. The reason are poor ice cloud parameterisations applying rough approximations to reality. These have provided sufficiently good results for a long time, as upper tropospheric relative humidity is hardly relevant to surface weather and thus used to be not of interest. It even took almost 100 years from the discovery of ice supersaturation in the atmosphere in 1906 (49) until it was introduced into an NWP model for the first time, namely the U.K. Meteorological Office Unified Model (51), and later also into the integrated forecast system (IFS) of the European Centre for Medium-Range Weather Forecasts (ECMWF, 47). Many models that nowadays incorporate ice supersaturation in one-moment ice cloud schemes apply a simplification termed "saturation adjustment" (29). This common practice allows ice supersaturation only in clear air, whereas the air inside clouds is assumed to be exactly saturated. Consequently, once nucleation occurs in highly supersaturated air, the entire supersaturation is transformed immediately into ice in the course of a single time step. This might be a reasonable approximation in strongly polluted air, where the number of ice crystals that are generated upon nucleation is large and thus the deposition of vapour is fast. However, upper tropospheric air usually tends to be relatively clean and thus cirrus clouds are often found in a state of ice supersaturation (32, 44, 3). As a result, the modelled upper tropospheric humidity fields, even though being broadly consistent with in-situ measurements (at least in the IFS, 18), feature a low-bias in the occurrence frequency and degree of ice supersaturation in the upper troposphere (10). Since this hampers a reliable prediction of flight routes that avoid the generation of strongly warming contrails, it is a crucial step on the way to sustainable air transportation to develop new parameterisations that treat upper tropospheric humidity in a more sophisticated way and produce more reliable forecasts of ice supersaturation on cruise levels.

In this thesis, a concept for such a parameterisation is proposed. A simple in-cloud humidity distribution is derived from simplifying assumptions in order to use the mean of this distribution in modelling the decay of the mean in-cloud humidity instead of adjusting it to exact saturation. It is furthermore acknowledged that this mean in-cloud humidity relaxes over time to an equilibrium supersaturation of a few percent rather than exact saturation, as long as the air is cooled continuously (19). The concept is developed within a stochastic box model representing one grid box of a 3D-model. Its implementation into a 3D-NWP model is left for future work.

The thesis is structured as follows: In the next chapter the development and functional principles of the models created during this work are explained. The newly developed parameterisations that are meant to replace saturation adjustment are tested in an artificial environment and compared to saturation adjustment in chapter 3. A discussion of the results and the applied simplifications is provided in chapter 4, before the thesis is summarized in chapter 5.

Chapter 2

Models

In the course of this thesis, four different models have been developed. The first one is a stochastic box model that simulates 10^4 air parcels representing one grid box of a NWP model. This model was used to simulate life cycles of simplified ice clouds and to study the humidity statistics inside them. It also served as a benchmark for reality to which the other models were compared. The second and third model are two versions of a new parameterisation for the treatment of ice clouds that explicitly model the decay of humidity inside the cloud and therefore should be an improvement to the practice of saturation adjustment. The fourth model is a parameterisation that represents the status quo in current NWP. It uses saturation adjustment and is meant to behave like the cirrus parameterisation currently implemented in the IFS at ECMWF. Note that in all models temperature changes are applied through adiabatic vertical motion only. Radiation effects and also latent heat have been neglected for the sake of simplicity. Also, pressure is always assumed constant throughout the simulations. The models are described in detail below.

2.1 Stochastic Box Model

As mentioned above, this model simulates 10^4 air parcels that represent one NWP model grid box. Each simulation is initiated in clear sky, i.e. the cloud fraction C and thus also the grid box mean specific ice water content q_i are zero in the beginning. In all parcels the temperature T is set to a common value which may at most be the supercooling limit of small droplets at about -38°C (24). This way, it is assured that any developing cloud later on can be assumed to consist of ice crystals only. The specific humidity q_p is initially uniformly distributed across the air parcels between $q_{\text{low}} := (1-a)q_{\text{init}}$ and $q_{\text{high}} := (1+a)q_{\text{init}}$, where $a < 1$ is a parameter to be chosen and q_{init} is the initial, mean, specific humidity in the considered clear sky air mass. Importantly, q_{init}, and thus also q_{high} and q_{low}, are constant values for a specific air mass. They always refer to the humidity distribution that the clear sky air mass used to have even if cloud formation was initiated.

Even though these settings are a strong simplification of the real sub-grid fluctuations in temperature and humidity (cf. 9), they have been implemented here, since they are in agree-

ment with the parameterisation in the current cycle of the IFS (7). Furthermore, these simplifications also come in handy, as they lead to a simple distribution of humidity inside a subsequently generated cloud (see below).

If now T decreases, the saturation specific humidity with respect to ice q_s which is calculated on the basis of the formula for the saturation vapour pressure of Murphy and Koop (31) is going to drop as well. Nevertheless, cloud formation will not be initiated if q_s passes q_{high}, as ice crystals are assumed to form by homogeneous nucleation only. The treatment of heterogeneous nucleation would involve the treatment of solid aerosol which is neglected in this first concept for the sake of simplicity. As Haag et al. (14) showed, this is generally not a bad approximation, since homogeneous nucleation is usually the dominant nucleation process in cirrus clouds. Therefore, cloud formation in this simple model only starts if the relative humidity with respect to ice RH_i in one of the air parcels passes the threshold for homogeneous nucleation specified by Kärcher and Lohmann (17):

$$RH_{\text{nuc}}(T) = 2.583 - \frac{T}{207.8\text{K}} \tag{2.1}$$

$$q_{\text{nuc}}(T) = RH_{\text{nuc}}(T)\, q_s(T) \tag{2.2}$$

From this time on, which is referred to as t_0, more and more air parcels will pass this nucleation threshold at their individual nucleation times $t_{\text{nuc}} \geq t_0$, as long as T keeps decreasing. Each of these air parcels is highly supersaturated at its individual nucleation event, when suddenly ice germs develop, and therefore the supersaturated water vapour begins to deposit on the ice crystals. While this process can be described in detail (cf. e.g. 24), the resulting rate at which humidity decays happens to be proportional to the current absolute supersaturation and thus it is parameterised here simply as

$$\frac{\mathrm{dq_p}}{\mathrm{dt}} = -\alpha(q_p(t) - q_s[T(t)]), \tag{2.3}$$

where α contains all the involved microphysical details (cf. 19, eq. 26). Its value is the larger the more ice surface is available for vapour deposition, either due to many ice crystals or due to large ice crystals. Eq. 2.3 describes an exponential decay of q_p towards q_s in every cloudy parcel from its individual t_{nuc} on, while the parcel's specific ice water content $q_{i,p}$ grows at the same rate, and after a small period of time δt we have

$$q_p(t + \delta t) = q_p(t) + \delta q_p \tag{2.4}$$

$$q_{i,p}(t + \delta t) = q_{i,p}(t) - \delta q_p, \qquad \text{where} \tag{2.5}$$

$$\delta q_p = -\alpha(q_p(t) - q_s(T))\, \delta t. \tag{2.6}$$

However, at the same time, q_s keeps decreasing as long as T continues its decrease. Hence, supersaturation is continuously restored inside the parcels and thus they will approach an equilibrium relative supersaturation S_{eq} (cf. e.g. 19, 20, 8), at which $\mathrm{dS/dt} = 0$. This

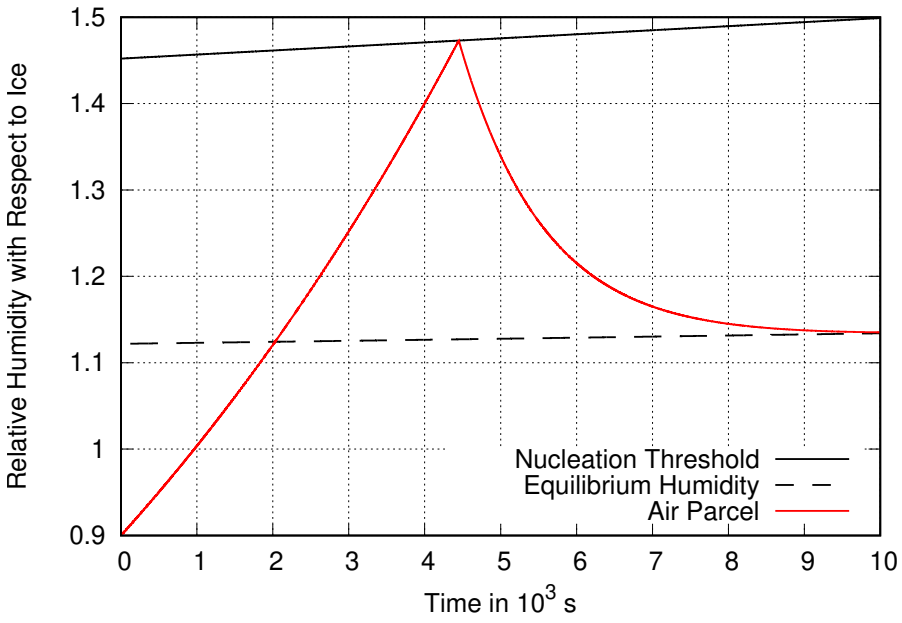

Figure 2.1: Example life cycle of an air parcel in a constant updraught of $10\,\mathrm{cm\,s^{-1}}$. The red curve shows the relative humidity of a single air parcel as it increases over time until it reaches the nucleation threshold (solid black). From there on, the supersaturation is consumed by depositional growth of ice crystals, which lowers the supersaturation down to an equilibrium value (dashed black) a few percent above saturation. Note that the equilibrium humidity is exaggerated here for the sake of clarity.

condition translates into:

$$0 = \left(\frac{\mathrm{dS}}{\mathrm{dt}}\right)_{\mathrm{eq}} = \frac{\mathrm{d}}{\mathrm{dt}}\left(\frac{q_p - q_s}{q_s}\right)_{\mathrm{eq}} \tag{2.7}$$

$$\frac{\mathrm{d\,ln\,q_p}}{\mathrm{dt}} = \frac{\mathrm{d\,ln\,q_s}}{\mathrm{dt}} \quad \text{in equilibrium,} \tag{2.8}$$

i.e. the relative rate, at which the specific humidity decreases due to the deposition of water vapour on ice crystals equals the relative rate, at which the saturation specific humidity decreases due to the cooling of the air. Using equation 2.3, S_{eq} can be written as

$$S_{\mathrm{eq}} = \left(\frac{\alpha}{-\mathrm{d\,ln\,q_s/dt}} - 1\right)^{-1}. \tag{2.9}$$

Apparently, it is not a priori clear that S_{eq} always exists. If the "deposition rate" α and the relative decrease rate of the saturation specific humidity approach each other, S_{eq} grows to $\pm\infty$. As the time scale for the deposition of water vapour is usually shorter than the time scale for cooling, this singularity requires slow deposition, i.e. few, small ice crystals, and strong cooling. Fortunately, the number of ice crystals grows quickly if cooling is strong since more and more aerosol particles are activated (17), and thus S_{eq} usually takes a value of a few percent above saturation. An example life cycle of one air parcel is provided in figure 2.1.

Since the individual air parcels begin their decay of humidity towards S_{eq} at different times t_{nuc}, their supersaturation at a given time is spread across a certain range. In order to

calculate the mean specific humidity inside the cloud in the new parameterisations (see below), a probability distribution $f_{S_p}(S)$ of the in-cloud supersaturation is needed. In principle, this can be fitted to a humidity histogram of all cloudy parcels in the stochastic box model, which may be necessary for more complicated initial conditions than assumed here. However, since q_p was uniformly distributed across the clear sky grid box in the considered case, an analytical expression for $f_{S_p}(S)$ can be derived.

Every air parcel starts its decay of supersaturation towards S_{eq} from the current nucleation threshold S_{nuc}. During a short time step, the change in temperature is small and thus also S_{eq} and S_{nuc} vary only little (cf. fig. 2.1) so that they can be assumed as constants for the sake of simplicity. The supersaturation S_p inside a single cloudy air parcel at a specific time $t_1 > t_{\mathrm{nuc}}$ is therefore approximated as

$$S_p(t_1, t_{\mathrm{nuc}}) = S_{\mathrm{eq}} + (S_{\mathrm{nuc}} - S_{\mathrm{eq}})\, e^{-\alpha\,(t_1 - t_{\mathrm{nuc}})} \tag{2.10}$$

so that young cloud parts ($t_{\mathrm{nuc}} \lesssim t_1$) are highly supersaturated, whereas old cloud parts ($t_{\mathrm{nuc}} \ll t_1$) show supersaturations close to the current S_{eq}. In order to derive $f_{S_p}(S)$, we start from the distribution $f_{t_{\mathrm{nuc}}}(t)$ of t_{nuc}, which is approximately uniform as long as $\mathrm{dq_s/dt}$ can be assumed as constant throughout the time step. Together with the time of the first nucleation event t_0, $f_{t_{\mathrm{nuc}}}(t)$ then reads

$$f_{t_{\mathrm{nuc}}}(t) = (t_1 - t_0)^{-1} \quad \text{for} \quad t \in [t_0;\, t_1]. \tag{2.11}$$

Further, eq. 2.10 gives a relation between nucleation at time t and supersaturation S at time t_1

$$\ln\left(\frac{S(t_1, t) - S_{\mathrm{eq}}}{S_{\mathrm{nuc}} - S_{\mathrm{eq}}}\right) = -\alpha(t_1 - t) \tag{2.12}$$

with the derivative

$$\frac{\mathrm{dt}}{\mathrm{dS}} = \frac{1}{\alpha(S(t_1, t) - S_{\mathrm{eq}})}. \tag{2.13}$$

By using the transformation law for probability densities, $f_{S_p}(S)$ can now be derived:

$$f_{S_p}(S) = f_{t_{\mathrm{nuc}}}[t(S)] \left|\frac{\mathrm{dt}}{\mathrm{dS}}\right| \tag{2.14}$$

$$= \frac{1}{\alpha\,(t_1 - t_0)\,(S - S_{eq})} \quad \text{for} \quad S \in [S_0, S_1], \tag{2.15}$$

where

$$S_0 = S_p(t_1, t_0) = S_{\mathrm{eq}} + (S_{\mathrm{nuc}} - S_{\mathrm{eq}})\, e^{-\alpha(t_1 - t_0)} \quad \text{and} \quad S_1 = S_p(t_1, t_1) = S_{\mathrm{nuc}}. \tag{2.16}$$

One can easily evaluate that $f_{S_p}(S)$ approaches a delta distribution centred at S_{eq} in the limit of a long time period between t_0 and the validation time t_1:

$$\lim_{t_1 \to \infty} f_{S_p}(S) = \delta(S - S_{\mathrm{eq}}) \tag{2.17}$$

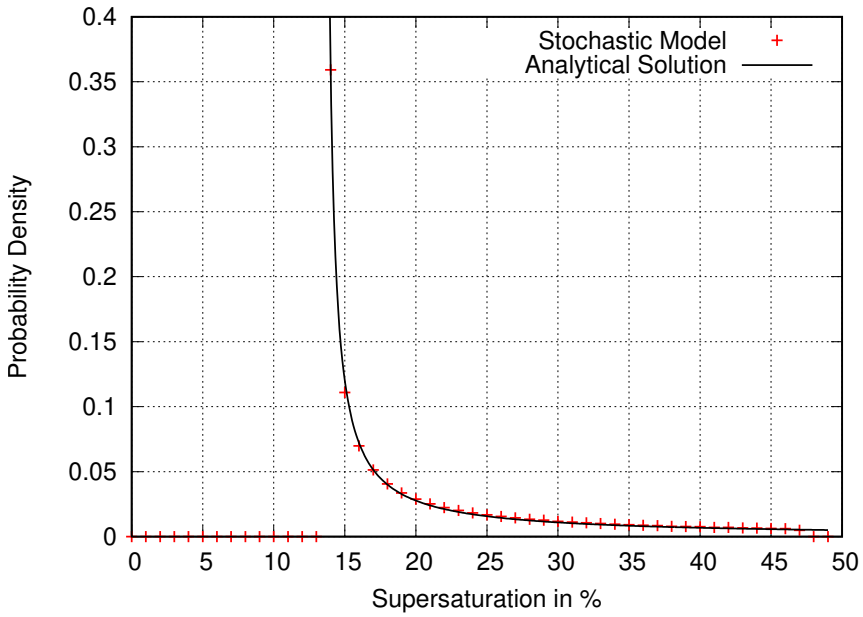

Figure 2.2: Hyperbolic distribution of supersaturation in the cloudy part of a grid box, analytical solution (solid line) and numerical result.

As long as cooling proceeds, this limit is still above saturation; an important difference to saturation adjustment. Note also that S_1 only equals S_{nuc} as long as nucleation continues. If cooling ceases, no new air parcels with $S_p = S_{\mathrm{nuc}}$ join the cloud any more and S_1 begins to evolve according to eq. 2.10, while the derived expression for the hyperbolic distribution of S_p remains valid.

Fig. 2.2 shows that the approximate analytic solution closely captures the probability distribution generated by the model in the case of a constant updraught despite the assumptions made. This changes in variable updraughts (not shown), because S_{eq} shows greater variability in this case and also the assumption of a uniform distribution of t_{nuc} collapses if the cooling rate varies in time. Hence, $f_{S_p}(S)$ will only be used for cloud parts that are newly generated within the current time step in the new parameterisations (see below).

2.2 Weak Adjustment

In order to improve the unphysical treatment of in-cloud humidity due to saturation adjustment, two different parameterisations that directly model the decay of the initially large supersaturation inside young cirrus clouds have been developed. The first one makes use of an adjustment in humidity similar to saturation adjustment, whereas the second one avoids adjusting humidity completely, but as a consequence requires the NWP model to memorize and process an additional prognostic variable. The starting point for the calculations are the prognostic variables for the considered grid box handed over by the core model to the parameterisation. In the case of the first new parameterisation these are the temperature T, the specific humidity q, the specific ice water content q_i and the cloud fraction C. Let

further δT be the change in T when integrating the next time step and recall that the grid box is considered to consist of an arbitrarily large number of air parcels. The objective for the parameterisation is then to estimate the values of the mentioned variables at the end of the current time step and hand them back over to the core model.

2.2.1 Initial Cloud Formation

The first case to consider is cooling air in clear sky, i.e. $\delta T < 0$ and $C = q_i = 0$. In this case, q_p is again assumed to be uniformly distributed between q_{low} and q_{high} across the grid box. If now temperature decreases, $q_s(T)$ and thus also $q_{\text{nuc}}(T)$ will drop as well and cloud formation is initiated if $q_{\text{nuc}}(T)$ is about to pass q_p at one point within the grid box, i.e. $q_{\text{nuc}} < q_{\text{high}} = (1+a)q_{\text{init}}$ by the end of the current time step. For the parameterisation this is the case if

$$q^n > \frac{q_{\text{nuc}}^{n+1}}{1+a}, \tag{2.18}$$

where upper indices n, $n+1$ label values at the boundaries of the current time step and thus $q_{\text{init}} = q^n$. The duration of one time step is denoted as $\Delta t = t^{n+1} - t^n$.

Due to the assumed uniform distribution of q_p and further assuming that q_{nuc} decreases linearly in the course of the time step, merely a simple geometrical consideration remains to determine the exact time t_0 of the first nucleation event and also the cloud fraction at the end of the time step. Specifically, the portion of the time step that it takes to reach t_0 from t^n is calculated as the remaining difference from q_{nuc} to q_{high} at the beginning of the time step divided by how much q_{nuc} changes during the whole time step:

$$t_0 = t^n + \Delta t \frac{q_{\text{nuc}}^n - q_{\text{high}}}{q_{\text{nuc}}^n - q_{\text{nuc}}^{n+1}} \tag{2.19}$$

Similarly, the generated cloud fraction can be calculated as the share of the total spread in humidity $q_{\text{high}} - q_{\text{low}} = 2aq_{\text{init}}$ that q_{nuc} has passed by the end of the time step:

$$C^{n+1} = \frac{q_{\text{high}} - q_{\text{nuc}}^{n+1}}{2a\, q_{\text{init}}} \tag{2.20}$$

In order to estimate the mean specific humidity q^{n+1}, the grid box is divided into the part that is going to be cloudy by the end of the time step and the part that remains clear. Having calculated t_0, the mean supersaturation inside the newly generated cloud at the end of the time step can be estimated as the mean of the humidity distribution f_{S_p} from eq. 2.15:

$$S_{\text{cl}}^{n+1} = \int_{S_0}^{S_1} S\, f_{S_p}(S)\, \mathrm{dS} \tag{2.21}$$

$$= S_{\text{eq}} + (S_{\text{nuc}} - S_{\text{eq}})\, \frac{1 - e^{-\alpha(t^{n+1} - t_0)}}{\alpha(t^{n+1} - t_0)} \tag{2.22}$$

$$q_{\text{cl}}^{n+1} = (S_{\text{cl}}^{n+1} + 1) q_s^{n+1} \tag{2.23}$$

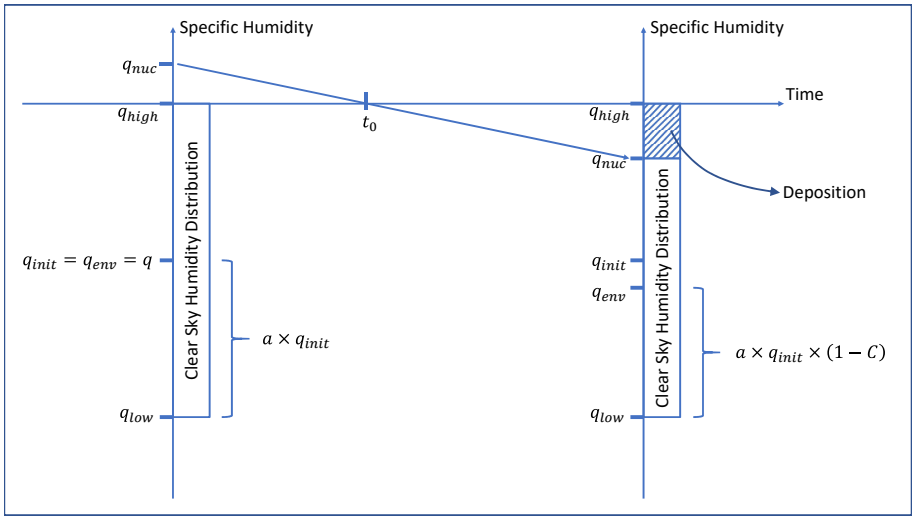

Figure 2.3: Schematic on the initiation of cloud formation in the parameterisation. At the time t_0, q_{nuc} propagates into the clear sky humidity distribution and thereby causes nucleation in the moistest part of the grid box. The parameterisation turns this part into a cloud and q_{nuc} becomes the new top end of the clear sky humidity distribution. The mean clear sky humidity q_{env} is adjusted accordingly.

S_{nuc} and S_{eq} do not vary a lot with temperature so that it does not make much difference, at which time within the time step these quantities are evaluated. In the simulations performed during this thesis, all calculations were carried out with their values at the beginning of the time step. As a quick check for plausibility, the two limits of eq. 2.22 are S_{eq} for large time differences $t^{n+1} - t_0$ and S_{nuc} for very small differences, as expected.

Determining the specific humidity q_{env} in the remaining clear sky environment of the cloud at the end of the time step is again a simple geometrical task. Before cloud formation, the total spread in humidity across the grid box was $2aq_{\mathrm{init}}$, which is reduced by a factor $1 - C^{n+1}$ by the end of the time step. q_{env}^{n+1} can then be calculated from q_{low} by adding half the current spread:

$$\begin{aligned} q_{\mathrm{env}}^{n+1} &= q_{\mathrm{low}} + a\, q_{\mathrm{init}}\, (1 - C^{n+1}) \\ &= q_{\mathrm{init}}\, (1 - a\, C^{n+1}) = q^n\, (1 - a\, C^{n+1}) \end{aligned} \tag{2.24}$$

Importantly, q_{init} and q_{high} remain unchanged, as they refer to the initial humidity distribution, before cloud formation commenced. Specifically, q_{high} is from now on not the top end of the clear sky humidity distribution any more and q_{init} is not its mean. Fig. 2.3 shows schematically, how the change in q_{nuc} affects the clear sky humidity distribution.

In case cloud formation was so vigorous that cloud fraction became unity within the time step of first nucleation (e.g. a small grid box with small a), q_{env}^{n+1} would be undefined and

the mean specific humidity at the end of the time step would simply equal q_{cl}^{n+1}. Otherwise, q^{n+1} is the weighted mean of q_{env}^{n+1} and q_{cl}^{n+1}

$$q^{n+1} = (1 - C^{n+1})\, q_{\mathrm{env}}^{n+1} + C^{n+1}\, q_{\mathrm{cl}}^{n+1} \tag{2.25}$$

so that the mean specific ice water content q_i^{n+1} can simply be derived from the continuity of the total water mass in the grid box:

$$q_i^{n+1} = q^n - q^{n+1} \tag{2.26}$$

Recall that the equations shown so far are valid only for the time step within which cloud formation commences. Equations for the following time steps are derived below.

2.2.2 Continual Cloud Growth

Now consider following time steps where still $\delta T < 0$ so that cloud formation is initiated in further parts of the grid box. The general time step ranges from t^{n+i} to t^{n+i+1}, $\quad i \geq 1$, but i is here taken as 1 without loss of generality. In the mean time, advection and sedimentation may likely have altered the values of the prognostic variables so that the start values T^{n+1}, q^{n+1}, q_i^{n+1} and C^{n+1} that are handed over to the parameterisation at the beginning of this time step do not equal the values computed in the last section, even though they are labelled identically.

In order to calculate the final values q_{env}^{n+2} and q_{cl}^{n+2} of this time step, it is necessary to first recalculate q_{env}^{n+1} and q_{cl}^{n+1} from the given prognostic variables, i.e. divide the now partly cloudy grid box into the cloudy and the clear sky part again. In principle, one can determine q_{env} at the beginning of the time step as in eq. 2.24, but first has to recover q_{init} since only q^{n+1} is currently in memory. Recall that q_{init}, and thus also q_{high} and q_{low}, are constant values for a specific air mass and refer to the initial clear sky humidity distribution, before cloud formation commenced. The desired q_{init} therefore does not equal the original q_{init} from the last section, since advection has likely changed the air mass contained by the grid box. Another approach would be to estimate q_{init} as the current total water content $q^{n+1} + q_i^{n+1}$ of the air mass currently filling the grid box, but, since ice may have sedimented out of or into the air mass, this is a bad approximation as well. q_{init} can rather be determined from how q_{nuc} propagates through the clear sky humidity distribution as cloud fraction increases. At the initiation of cloud formation, q_{nuc} equals q_{high}. As the cloud grows larger and larger, q_{nuc} propagates through the entire clear sky humidity spread $2aq_{\mathrm{init}}$, before it reaches q_{low} when the cloud fraction becomes unity. Because of our assumption of a uniform distribution of the humidity fluctuations, this propagation is linear in C and we have

$$q_{\mathrm{nuc}}(C) = q_{\mathrm{high}} - 2aq_{\mathrm{init}}C = (1 + a)q_{\mathrm{init}} - 2aq_{\mathrm{init}}C \tag{2.27}$$

so that q_{init} may always be recovered as

$$q_{\text{init}} = \frac{q_{\text{nuc}}}{1 + a - 2aC}. \tag{2.28}$$

Combining this with eq. 2.24, q_{env} at the beginning of the current time step may be calculated as

$$q_{\text{env}}^{n+1} = q_{\text{init}} \left(1 - a\, C^{n+1}\right) \tag{2.29}$$

$$= \frac{1 - aC^{n+1}}{1 + a - 2aC^{n+1}} q_{\text{nuc}}^{n+1}. \tag{2.30}$$

q_{cl}^{n+1} can then be determined by simply rearranging eq. 2.25:

$$q_{\text{cl}}^{n+1} = \frac{q^{n+1} - (1 - C^{n+1}) q_{\text{env}}^{n+1}}{C^{n+1}} \tag{2.31}$$

The increase in cloud fraction and the clear sky specific humidity at the end of the time step may now be calculated as in eqs. 2.20 and 2.24 by inferring q_{init} according to eq. 2.29:

$$C^{n+2} = C^{n+1} + \Delta C, \quad \text{where} \tag{2.32}$$

$$\Delta C = \frac{q_{\text{nuc}}^{n+1} - q_{\text{nuc}}^{n+2}}{2a q_{\text{init}}} = (q_{\text{nuc}}^{n+1} - q_{\text{nuc}}^{n+2}) \frac{1 - a\, C^{n+1}}{2a\, q_{\text{env}}^{n+1}} \tag{2.33}$$

$$q_{\text{env}}^{n+2} = q_{\text{init}} \left(1 - a\, C^{n+2}\right) = q_{\text{env}}^{n+1} \frac{1 - a\, C^{n+2}}{1 - a\, C^{n+1}} \tag{2.34}$$

In order to determine the in-cloud humidity at the end of the time step, the grown cloud is split into the old part with cloud fraction C^{n+1} and the new part with cloud fraction ΔC. In the new part, cloud formation is initiated according to eqs. 2.21 to 2.23 as if a new cloud was developed right from the beginning of the time step, i.e. $t_0 = t^{n+1}$:

$$S_{\text{new}} = S_{\text{eq}} + (S_{\text{nuc}} - S_{\text{eq}}) \frac{1 - e^{-\alpha\, \Delta t}}{\alpha\, \Delta t} \tag{2.35}$$

$$q_{\text{new}} = (S_{\text{new}} + 1) q_s^{n+2} \tag{2.36}$$

To the contrary, the old cloud part can be considered as an individual cloud that stopped growing at t^{n+1}. In principle, one could still use the probability distribution f_{S_p} from eq. 2.15, but with the upper bound S_1 no longer equal to S_{nuc}. Since no new, highly supersaturated air parcels join this part of the cloud any more, S_1 would begin to decay in time as $S_p(t,\, t^{n+1})$ according to eq. 2.10 analogously to the lower boundary S_0 of the distribution so that the mean supersaturation in the old cloud part could be estimated as

$$S_{\text{old}} = \int_{S_p(t^{n+2},\, t_0)}^{S_p(t^{n+2},\, t^{n+1})} S\, f_{S_p}(S)\, \mathrm{dS} \tag{2.37}$$

$$= S_{\text{eq}} + (S_{\text{nuc}} - S_{\text{eq}}) \frac{\left(e^{\alpha t^{n+1}} - e^{\alpha t_0}\right) e^{-\alpha\, t^{n+2}}}{\alpha (t^{n+1} - t_0)}. \tag{2.38}$$

However, as already mentioned before, the assumptions made in the derivation of f_{S_p} become increasingly worse the greater the difference between t_0 and t^{n+1} gets. Additionally, t_0 would have to be estimated from q_{cl}^{n+1} first in order to evaluate eq 2.38. Instead, one recalls that all quantities in eq. 2.38 are constant or show little variation in time so that S_{old} can be approximated to decay exponentially in t^{n+2} towards S_{eq}. This result might be expected for the mean humidity if the humidity decays exponentially in all the individual air parcels. The average specific humidity in the old cloud part is thus simply evolved as

$$q_{\mathrm{old}} = q_{\mathrm{cl}}^{n+1} - \alpha\,\Delta t(q_{\mathrm{cl}}^{n+1} - q_s^{n+1}). \tag{2.39}$$

The average specific humidity in the whole cloud is then the weighted mean of q_{old} and q_{new}

$$q_{\mathrm{cl}}^{n+2} = \frac{C^{n+1}}{C^{n+2}} q_{\mathrm{old}} + \frac{\Delta C}{C^{n+2}} q_{\mathrm{new}} \tag{2.40}$$

and the grid box mean humidity is, as before, the weighted mean of q_{cl}^{n+2} and q_{env}^{n+2} (cf. eq. 2.25). Finally, the loss in vapour is added to the ice mass:

$$q_i^{n+2} = q_i^{n+1} + (q^{n+1} - q^{n+2}) \tag{2.41}$$

2.2.3 Continual Cloud Growth to Full Coverage

If cooling proceeds over a longer period of time, q_{nuc} is eventually going to pass q_{low}, i.e. overcast conditions are about to be reached in the course of the current time step. It is then necessary to record the exact time t_1, when this happens, which is again achieved by a geometrical consideration. Let the current time step begin at t^m. The clear sky specific humidity q_{env}^m can again be calculated according to eq. 2.30. The portion of the time step that it takes to reach full coverage can then be estimated as the remaining spread in clear sky humidity divided by how much q_{nuc} changes during the entire time step:

$$t_1 = t^m + \Delta t \frac{2(q_{\mathrm{nuc}}^m - q_{\mathrm{env}}^m)}{q_{\mathrm{nuc}}^m - q_{\mathrm{nuc}}^{m+1}} \tag{2.42}$$

The average humidity in the new cloud part at the end of the time step is now computed in two steps. During the first step from t^m to t_1, the upper boundary of f_{S_p} is still S_{nuc} so that the new cloud part can be treated as usual, which gives a preliminary supersaturation S_{new}^* at t_1:

$$S_{\mathrm{new}}^* = S_{\mathrm{eq}} + (S_{\mathrm{nuc}} - S_{\mathrm{eq}})\,\frac{1 - e^{-\alpha(t_1 - t^m)}}{\alpha(t_1 - t^m)} \tag{2.43}$$

$$q_{\mathrm{new}}^* = (S_{\mathrm{new}}^* + 1)\,q_s^m \tag{2.44}$$

When nucleation ceases, i.e. at t_1, the new cloud part stops growing, since no more clear sky is left within the grid box. From this time on, this cloud part can thus be treated like the

old one:

$$q_{\text{new}} = q^*_{\text{new}} - \alpha(t^{m+1} - t_1)(q^*_{\text{new}} - q^m_s) \tag{2.45}$$

q_{old} can simply be calculated as before so that the grid mean humidity becomes

$$q^{m+1} = C^m\, q_{\text{old}} + (1 - C^m)\, q_{\text{new}}. \tag{2.46}$$

C can then be set to one and q_i^{m+1} is computed according to eq. 2.41.

2.2.4 Cooling in overcast skies

If cooling proceeds in already overcast conditions in a time step t^{m+i} to t^{m+i+1}, where again $i = 1$ without loss of generality, the whole cloud cannot grow further and thus q simply decays analogously to eq. 2.39

$$q^{m+2} = q^{m+1} - \alpha\, \Delta t(q^{m+1} - q_s^{m+1}) \tag{2.47}$$

and the increase in ice mass is, as before, derived according to eq. 2.41.

2.2.5 Warming in overcast skies

So far, only $\delta T < 0$ has been considered. Now, consider a time step t^k to t^{k+1}, during which $\delta T > 0$ and $C = 1$, i.e. warming in overcast skies. If temperature keeps rising for a longer period of time, q_s will rise beyond q_p in more and more air parcels, in which case the ice crystals in these parcels are expected to sublimate and eventually vanish. In contrast to cloud formation, this is a rather slow process, since there is no large difference between q_p and q_s in this case as there was at the moment of nucleation. Hence, only small amounts of ice sublimate per time step and therefore one would have to set a threshold for $q_{i,p}$, below which there is such little ice left in a parcel that it can be considered as no longer cloudy. This is not the topic of this thesis and thus all parcels are simply assumed to remain cloudy in this first concept, until there is no more ice left in the entire grid box, i.e. $C = 1$ as long as $q_i > 0$.

This means that again everything that has to be computed by the parameterisation is the approach of q to q_s and the corresponding change in ice mass. In contrast to the previous section though, the difference between q^k and q_s^k may become negative if warming proceeds over a longer period of time so that q no longer decreases due to deposition but increases due to sublimation. Nevertheless, eqs. 2.47 and 2.41 still hold for q^{k+1} and q_i^{k+1}, respectively. However, if sublimation continues for multiple time steps, the change in q might cause q_i^{k+1} to become negative. If this is the case, the cloud is about to vanish in the course of the time step, and eqs. 2.47 and 2.41 have to be replaced by

$$q^{k+1} = q^k + q_i^k \tag{2.48}$$

$$q_i^{k+1} = 0 \tag{2.49}$$

$$C^{k+1} = 0. \tag{2.50}$$

2.2.6 Warming in partially cloudy skies

Finally, the change in the prognostic variables has to be determined for the case of $\delta T > 0$ in partially cloudy skies. For this purpose now assume that $0 < C < 1$ during the time step from t^k to t^{k+1}. Since cloud edge erosion is neglected in this first concept, C is again assumed to remain constant until all ice has sublimated.

A major complication now arises from the fact that the grid box again has to be divided into the cloudy and the clear sky part, but eq. 2.30 no longer holds for q_{env}^k. The reason is that q_{nuc}^k rises with temperature and thus is not the upper boundary of the clear sky humidity distribution any more. Thus, q_{nuc}^k can no longer be used as an anchor, to which the clear sky humidity distribution can be attached. In order to still be able to divide the grid box into the cloudy and the clear sky part, S_{cl} is adjusted to S_{eq} in this situation.

As a first step, one needs to check, whether the considered time step is the first one under warming conditions, since this determines, whether S_{cl} has already been adjusted in earlier time steps. For this purpose, the parameterisation at first assumes every time step to be the first one under warming conditions, in which case q_{nuc}^k is still the upper boundary of the clear sky humidity distribution and thus eqs. 2.30 and 2.31 are still valid for q_{env}^k and q_{cl}^k, respectively. Especially, q_{cl}^k will be larger than q_s^k, if temperature has been decreasing during the previous time steps.

However, if this is not the first time step with $\delta T > 0$, the warming in previous time steps will have risen q_{nuc}^k away from the actual clear sky humidity distribution and thus still using it to compute q_{env}^k according to eq. 2.30 will give a too large value. Accordingly, the calculated value for q_{cl}^k will be too low, especially lower than q_s^k, since the in-cloud humidity has already been adjusted to S_{eq} in this case and $S_{\mathrm{eq}} < 0$ under warming conditions (cf. eq. 2.9).

This means one can easily check, whether q_{cl}^k should rather be estimated by using eq. 2.31 or be set to $(S_{\mathrm{eq}} + 1)q_s^k$, by simply evaluating whether the value computed via eq. 2.31 is above or below saturation. If the value from eq. 2.31 is below saturation, it is wrong, since the current time step is then not considered the first one under warming conditions and q_{env}^k was thus derived from wrong assumptions. The in-cloud humidity then has already been adjusted to S_{eq} previously and q_{cl}^k is better estimated as

$$q_{\mathrm{cl}}^k = (S_{\mathrm{eq}} + 1)q_s^k. \tag{2.51}$$

However, if the value from eq. 2.31 is larger than saturation, it can be assumed to be the correct value and the humidity in the cloud still needs to be adjusted to the value from eq. 2.51, since the current time step then is considered the first under warming conditions. This is done by transforming the excess water vapour in the cloudy part of the grid box immediately into ice, similar to saturation adjustment, which gives preliminary specific water contents q^{k*}

and q_i^{k*}

$$q^{k*} = q^k + \delta q^* \tag{2.52}$$

$$q_i^{k*} = q_i^k - \delta q^*, \quad \text{where} \tag{2.53}$$

$$\delta q^* = C^k (q_{\mathrm{cl}}^{k*} - q_{\mathrm{cl}}^k), \tag{2.54}$$

with q_{cl}^{k*} computed according to eq. 2.51.

This treatment of in-cloud humidity must be tested under realistic conditions with great caution. The actual value of q_{cl}^k may likely be in between the two estimates, as advection may have mixed air masses from already adjusted grid boxes with air masses from not yet adjusted grid boxes. Also, eq. 2.51 unfortunately may likely give a bad estimate if δT changes significantly between the time steps. The reason is that S_{eq} depends on δT via the derivative of q_s so that the S_{eq} that the cloud has been adjusted to at the end of the last time step usually does not equal the S_{eq} in eq. 2.51, even if advection is neglected. These two issues may lead to unphysical sub grid fluxes of humidity between the cloudy and the clear sky part of the grid box (cf. 47), since they are connected via q^k and thus an underestimation of the one specific humidity leads to an overestimation of the other. These fluxes consequently may lead to deviating estimates of the sublimation rate of the ice crystals. Fortunately, the considered cloud would likely have undergone a period of very weak cooling, before the cooling reversed into warming, so that the in-cloud humidity would have relaxed to S_{eq} quite far already anyway. Therefore, both the adjustment itself and the mentioned errors should usually be minor.

Regardless of whether the current time step is the first one under warming conditions or not, the specific humidity in the grid box has to be increased according to the adjustment of the in-cloud humidity due to the increase in temperature in the course of the time step

$$\delta q = C^k (q_{\mathrm{cl}}^{k+1} - q_{\mathrm{cl}}^{k(*)}), \tag{2.55}$$

where q_{cl}^{k+1} is also computed according to eq. 2.51 with q_s^{k+1} instead of q_s^k. As already mentioned, $q_{\mathrm{cl}}^{k(*)}$ may likely be a bad estimate for the value at the beginning of the time step. Hence, δq might be too large if δT is now larger than it was in the previous time step or too small if δT is smaller than before. During the early time steps of a warming period, when δT increases from time step to time step, the resulting too large increase in q can be limited, since it leads to unrealistically high values of q_{env}, which can be diagnosed. As, in this case, the cooling period that created the cloud is not that long ago, the difference between q_{nuc}^k and the top of the clear sky humidity distribution is not yet that large and thus eq. 2.30 still gives a reasonable, though slightly too high, estimate for q_{env}^k. Since the specific humidity in the cloud environment inside the air mass should not change under warming conditions, the value from eq. 2.30 can be considered an upper limit for q_{env}^k. The parameterisation thus calculates, what q_{env}^{k+1} would become if δq from eq. 2.55 was added to q^k as

$$q_{\mathrm{env}}^{k+1} = \frac{q^k + \delta q - C^k\, q_{\mathrm{cl}}^{k+1}}{1 - C^k} \tag{2.56}$$

and if this value is larger than the limit set by eq. 2.30, it simply discards δq from eq. 2.55 and instead calculates q^{k+1} according to eq. 2.25 using q^k_{env} from eq. 2.30 and q^{k+1}_{cl}. Recall that in this case $C^{k+1} = C^k$. If, however, q^{k+1}_{env} from eq. 2.56 is below the limit set by eq. 2.30, then δq is the better estimate for the change in specific humidity and thus the parameterisation calculates

$$q^{k+1} = q^k + \delta q \tag{2.57}$$

$$q_i^{k+1} = q_i^k - \delta q. \tag{2.58}$$

This, though, again is only executed as long as $q_i^k > \delta q$. If ice sublimation has proceeded so far that $q_i^k < \delta q$, the cloud is about to vanish in the course of the current time step, in which case, as before, eqs. 2.48 to 2.50 are executed.

2.3 No Saturation Adjustment

The complications described in the previous section about the warming in partially cloudy skies and the need for an adjustment of in-cloud humidity arise from the lack of information about q_{env} and q_{cl}. In cooling environments, this is not a problem, since the clear sky humidity distribution can then be linked to q_{nuc} and is therefore no longer unknown. Hence, it would in principle suffice to memorize one of these two average specific humidities from the previous time step in every partly cloudy grid box that undergoes warming in order to overcome humidity adjustment entirely. Unfortunately, one does not know, which grid boxes are going to experience warming during the next time step, when calculating the current. It is therefore necessary to introduce a complete new prognostic variable into the NWP model that is advected around and memorized for every cloudy grid box. In this case, q_{cl} was chosen to be this variable. Apart from a much simpler computation under warming conditions, this has the benefit that also during cooling q_{env} does not have to be calculated according to eq. 2.30, but can be retrieved from q, q_{cl} and C via rearranging eq. 2.25

$$q^k_{\mathrm{env}} = \frac{q^k - C^k\, q^k_{\mathrm{cl}}}{1 - C^k}, \tag{2.59}$$

and q^k_{cl} obviously does not have to be computed at all any more.

Additionally, one no longer has to distinguish between full coverage and partly cloudy skies during warming. In any case, the cloud is no longer growing and thus its humidity simply decays exponentially towards saturation analogously to eq. 2.47

$$q^{k+1}_{\mathrm{cl}} = q^k_{\mathrm{cl}} - \alpha\, \Delta t (q^k_{\mathrm{cl}} - q^k_s), \tag{2.60}$$

while the clear sky humidity (if any) remains unchanged. Hence, the parameterisation then only computes δq according to eq. 2.55 with the now explicitly decaying q^{k+1}_{cl} and uses this to derive q^{k+1} and q_i^{k+1} as before.

2.4 Saturation Adjustment

This parameterisation was programmed according to ECMWF (7). Nevertheless, it will not behave exactly like the currently implemented parameterisation in the IFS, since some details had to be inferred and also cloud edge erosion is neglected, in order to keep it comparable to the new parameterisations. The differences to the new parameterisations will be explained below.

2.4.1 Initial Cloud Formation

At the onset of cloud formation in the time step t^n to t^{n+1}, there is no need to compute the exact time of first nucleation. Also, q_{cl} does not have to be calculated, since it is simply q_s. As can be seen in the previous section, it is also unnecessary to compute q_{env} from geometric considerations if q_{cl} is always known, since it can simply be calculated from eq. 2.59. Instead, the change in specific humidity is calculated in two steps. The first of these is to bring all air parcels, in which q_{nuc} passes q_p within the time step, back down to q_{nuc}^{n+1}. As the air parcels have differing specific humidities at the beginning of the time step, the difference to q_{nuc}^{n+1} varies between $q_{\mathrm{high}} - q_{\mathrm{nuc}}^{n+1}$ for the most humid air parcels and 0 for those, that nucleated right at the end of the time step. Due to the assumption of a uniform humidity distribution in clear sky, the mean of these differences across the nucleating parcels is simply the arithmetic mean of these two extremes such that the change in specific humidity due to this first adjustment is

$$\delta q_1 = -\frac{q_{\mathrm{high}} - q_{\mathrm{nuc}}^{n+1}}{2}\Delta C \tag{2.61}$$

The second step is then the actual adjustment to saturation

$$\delta q_2 = -(q_{\mathrm{nuc}}^{n+1} - q_s^{n+1})\Delta C \tag{2.62}$$

so that q^{n+1} and q_i^{n+1} are calculated as

$$q^{n+1} = q^n + \delta q_1 + \delta q_2 \tag{2.63}$$

$$q_i^{n+1} = -\delta q_1 - \delta q_2. \tag{2.64}$$

The calculation of cloud fraction is equivalent to the one used in the new parameterisations.

2.4.2 Continual Cloud Life Cycle

Now, again consider subsequent time steps, e.g. t^{n+1} to t^{n+2}. If cooling proceeds, q_{high} has to be replaced by q_{nuc}^{n+1} in the derivation of δq_1, since this is then the top end of the clear sky humidity distribution at the beginning of the time step:

$$\delta q_1 = -\frac{q_{\mathrm{nuc}}^{n+1} - q_{\mathrm{nuc}}^{n+2}}{2}\Delta C \tag{2.65}$$

Additionally, there is a third deposition term that accounts for the adjustment of the old cloud to the saturation specific humidity at the new temperature

$$\delta q_3 = -(q_s^{n+1} - q_s^{n+2})C^{n+1} \tag{2.66}$$

so that q^{n+2} and q_i^{n+2} are evaluated as

$$q^{n+2} = q^{n+1} + \delta q_1 + \delta q_2 + \delta q_3 \tag{2.67}$$

$$q_i^{n+2} = q_i^{n+1} - \delta q_1 - \delta q_2 - \delta q_3. \tag{2.68}$$

If cooling reverses into warming, the terms δq_1 and δq_2 vanish, since they only correspond to newly generated cloud parts. Hence, only δq_3 has to be added in this case in order to model the sublimation of the ice crystals. If this causes q_i^{n+2} to become negative, the cloud vanishes and eqs. 2.48 to 2.50 are once again valid instead.

2.4.3 Continual Cloud Growth to Full Coverage

In a time step t^m to t^{m+1}, during which ongoing cooling leads to overcast conditions, it is again unnecessary to evaluate the exact time when this happens or even to compute any of the above δqs, since q^{m+1} simply becomes q_s^{m+1}:

$$q^{m+1} = q_s^{m+1} \tag{2.69}$$

$$q_i^{m+1} = q_i^m + (q^m - q_s^{m+1}) \tag{2.70}$$

$$C^{m+1} = 1 \tag{2.71}$$

These equations also hold for following time steps, in which cooling proceeds in overcast skies.

Chapter 3

Results

Several idealistic simulations have been run, in which the three parameterisations compete in following the behaviour of the stochastic box model as closely as possible, since this model serves as a benchmark for reality in this first concept study. Table 3.1 gives an overview of the performed simulations. Two different vertical wind scenarios are considered, one with a constant updraught ("const" in table 3.1) and one where the vertical wind $w(t)$ follows half a period of a cosine function that changes amplitude half way through the simulation ("cos" in table 3.1). In the further simulations, these two scenarios are combined with variations of other parameters, in particular α, a and Δt, in order to test the sensitivity of the parameterisations to variations of these parameters. All tests are illustrated with pairs of figures, where the right panel always shows the temporal evolution of the in-cloud relative humidity, which is closely related to the new prognostic variable that was introduced in the no-adjustment parameterisation and thus is a variable commonly not used within the rest of NWP models so far. The left panel always shows the temporal evolution of the grid box mean relative humidity, which is the quantity that is more relevant to numerical weather prediction.

If not noted differently, a has a value of 0.25 in all the experiments such that nucleation is initiated if $q > \frac{q_{\mathrm{nuc}}}{1+0.25} = 0.8\, q_{\mathrm{nuc}}$, which is the current standard in the IFS. The value for the deposition rate α, which is $3 \cdot 10^{-4}\mathrm{s}^{-1}$ in most experiments, was obtained by taking into account the results of Khvorostyanov and Sassen (20). According to their table A1, this value

Table 3.1: Overview of the tests

Wind scenario	$w(t)$ (cm/s)	α (1/s)	a	Δt (s)
Scenario 1 (Fig. 3.1)	const (2)	$3 \cdot 10^{-4}$	0.25	60
Scenario 2 (Fig. 3.2)	cos	$3 \cdot 10^{-4}$	0.25	60
Scenario 1 (Fig. 3.3)	const (2)	$2.8 \cdot 10^{-3}$	0.25	60
Scenario 2 (Fig. 3.4)	const (2)	$2.8 \cdot 10^{-3}$	0.25	60
Scenario 1 (Fig. 3.5)	const (2)	$3 \cdot 10^{-4}$	0.10	60
Scenario 2 (Fig. 3.6)	cos	$3 \cdot 10^{-4}$	0.10	60
Scenario 1 (Fig. 3.7)	const (10)	$3 \cdot 10^{-4}$	0.25	60
Scenario 1 (Fig. 3.8)	const (2)	$3 \cdot 10^{-4}$	0.25	600
Scenario 2 (Fig. 3.9)	cos	$3 \cdot 10^{-4}$	0.25	600

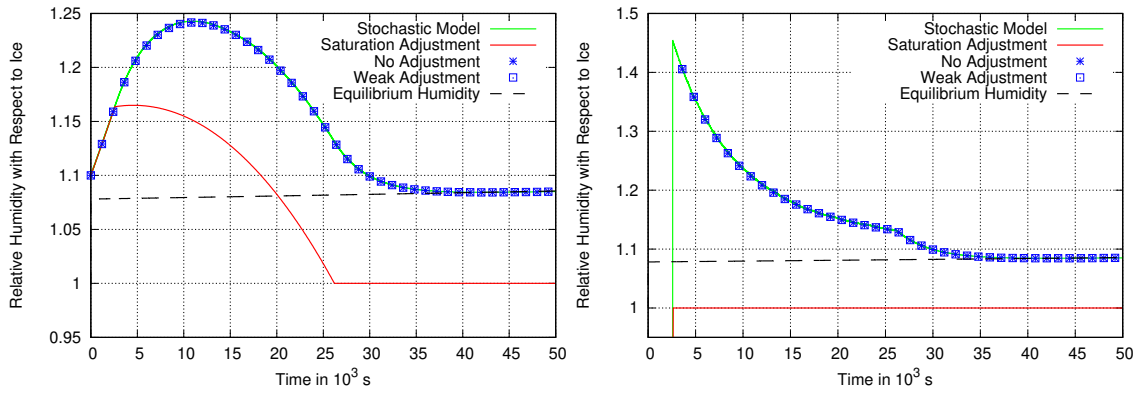

Figure 3.1: Scenario 1: Left panel: Grid box mean relative humidity (with respect to ice) as a function of time in a grid box that undergoes cooling in a constant updraught of $2\,\mathrm{cm\,s^{-1}}$ and cloud formation with $\alpha = 3 \cdot 10^{-4}\,\mathrm{s^{-1}}$. Shown is the behaviour of the stochastic box model that treats one grid box as an ensemble of 10^4 air parcels with an initial distribution of specific humidity (green); this model is assumed to best represent reality and serves as a benchmark for the parameterisations. The new parameterisations (blue marks) follow the stochastic model closely, while the parameterisation that uses saturation adjustment (red) does not, which leads to an underestimation of the mean relative humidity and thus of supersaturation. The new parameterisations approach the equlibrium supersaturation (black dashed), while saturation adjustment assumes exactly saturation inside the cloud. Right panel: The corresponding mean in-cloud relative humidity for the stochastic model, the new parameterisations, and the adjustment parameterisation. One can clearly see, how the decay of humidity in the stochastic box model changes into a pure exponential, once the cloud fraction reaches unity and no new, highly supersaturated cloud parts join the cloud anymore.

for example corresponds to the deposition of water vapour on about 100 ice crystals with a mean radius of 10μm per litre of air. While the stochastic box model works with a time step of one second, it was chosen to be 60s in the parameterisations if not noted differently. Furthermore, all simulations start from a grid box mean relative humidity with respect to ice of 110% and a grid box mean temperature of 235K, which is about the limiting temperature for the supercooling of small droplets. This way, it is assured that, when nucleation occurs after a period of cooling, the resulting cloud can be considered to consist of ice particles only. Finally, all experiments are initiated in clear sky, i.e. $C = q_i = 0$.

In a first simple experiment, constant cooling is applied throughout the simulation in the form of an updraught of $2\,\mathrm{cm\,s^{-1}}$. Fig. 3.1 shows the resulting grid box mean and in-cloud mean relative humidities with respect to ice as functions of time. Obviously, the two new parameterisations produce the exact same output, since they only differ under warming conditions in partly cloudy skies. They both closely follow the behaviour of the stochastic box model and thus show great improvement in comparison with saturation adjustment. Besides that, this experiment illustrates well that the underestimation of supersaturation in cloudy situations resulting from saturation adjustment is twofold. First, the sudden condensation of large amounts of water vapour begins to drive the grid mean humidity down to saturation soon after the first nucleation event. To the contrary, the actual, slow initiation of the condensation process first leads to a further increase in relative humidity, until the cloudy

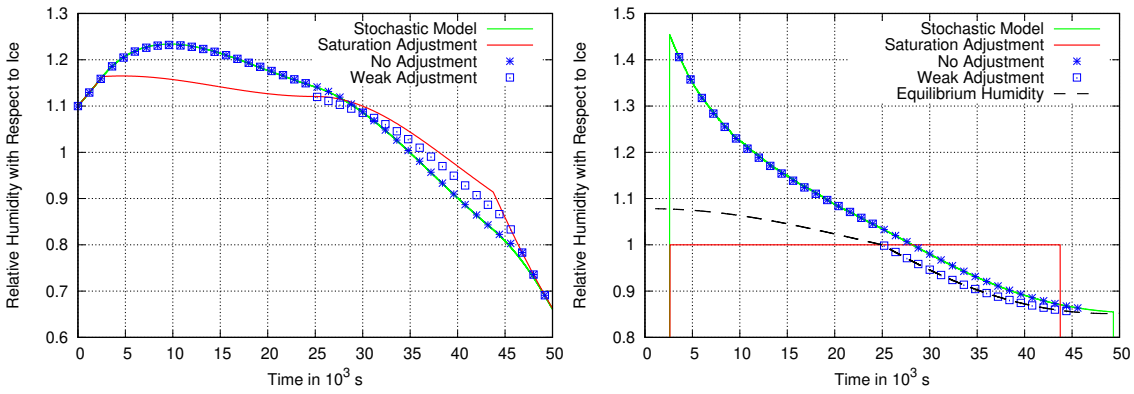

Figure 3.2: Scenario 2: Left and right panels: as left and right panels of Fig. 3.1, but for a situation that starts with cooling and ends with heating. The temperature change is applied through vertical wind in the form of half a period of a cosine function in time with an amplitude that changes half way through the simulation from $2\,\mathrm{cm\,s^{-1}}$ to $5\,\mathrm{cm\,s^{-1}}$.

portion of the grid box has grown large enough to compensate the rise in relative humidity in the remaining clear sky part of the grid box. Secondly, the relative humidity in the case of saturation adjustment becomes exactly 100%, once the cloud fraction reaches unity, whereas in fact the continuous cooling keeps restoring the supersaturation so that even after long time periods the cloud remains in a slightly supersaturated state.

In the second experiment, the temperature change was modified with a time dependence. The simulation begins with cooling through an updraught of $2\,\mathrm{cm\,s^{-1}}$ which then decelerates in the form of a cosine function until it vanishes half way through the simulation. At this point, when the cooling reverses into warming, the cosine changes its amplitude so that the experiment ends in a downdraught of $5\,\mathrm{cm\,s^{-1}}$. Fig. 3.2 again shows the grid box mean and the in-cloud mean relative humidities for this case as functions of time. The stochastic model clearly shows, how the in-cloud supersaturation quickly reverses into subsaturation after the onset of warming, since the sublimation of the ice particles cannot restore saturation instantaneously. The parameterisation without humidity adjustment proves to be very well capable of representing this in-cloud subsaturation and still follows the stochastic model closely, as it simply approaches S_{eq} exponentially, which becomes negative under warming conditions (cf. eq. 2.9). Since the cloud fraction does not reach unity by the end of the cooling period, the subsequent warming period takes place in partly cloudy skies and consequently the weak adjustment parameterisation has to adjust its in-cloud humidity right at the onset of warming. Note though that it still stays closer to the stochastic box model than the saturation adjustment parameterisation, since the in-cloud humidity in this case is adjusted to the equilibrium value S_{eq} rather than exact saturation. Nevertheless, the weak adjustment method still overestimates the grid box mean relative humidity soon after the warming period has started, even though it slightly underestimates the mean in-cloud humidity. This is a consequence of the earlier mentioned sub-grid humidity flux, which is caused by the change in ΔT from time step to time step. This flux leads to an increase in clear sky specific humidity (not shown), which explains the overestimation of the grid box mean humidity.

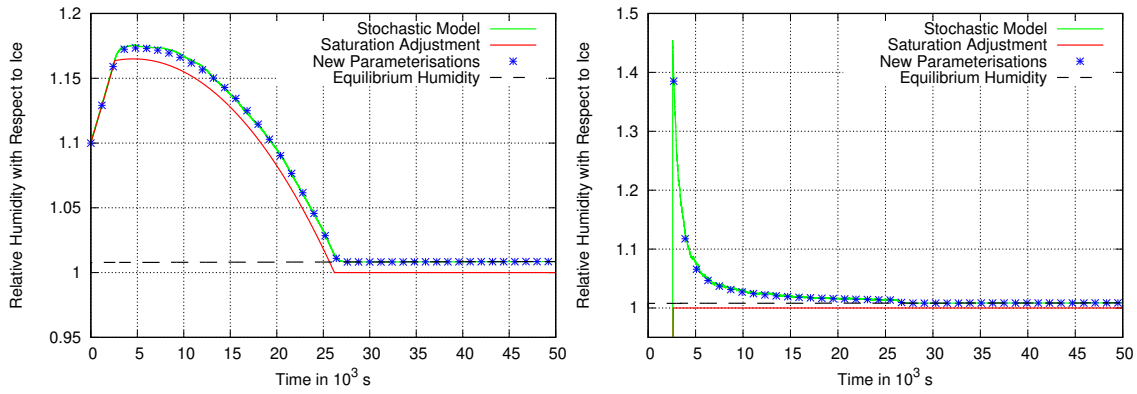

Figure 3.3: Scenario 1, but with $\alpha = 2.8 \cdot 10^{-3}$ s^{-1}, which corresponds to a cloud with 1000 crystals of 10 μm radius per litre.

Concerning the time of cloud dispersal, one can observe that the cloud survives longer the slower the sublimation process is modelled. In saturation adjustment, large amounts of water vapour have to be converted from the ice phase every time step in order to maintain saturated conditions inside the cloud. Consequently, the ice mass is soon depleted and the cloud vanishes most quickly in this parameterisation. The weak adjustment parameterisation assumes the largest in-cloud subsaturation, by simply adjusting the in-cloud humidity to its equilibrium value. This means that the amount of ice that has already sublimated to restore the in-cloud relative humidity at a specific point in time is the smallest in this parameterisation and thus the sublimation process should be the slowest among the three parameterisations. However, this parameterisation continuously sublimates too large amounts of ice in the accelerating downdraught and shifts the additional water vapour from the cloud into the clear sky environment. The ice mass is therefore depleted second fastest in this parameterisation. The parameterisation without humidity adjustment captures the sublimation process very well, until the first air parcels in the stochastic model become ice free. From this point on, the sublimation process in the stochastic model slows down, since the air parcels, in which the remaining ice is still converted, become less and less. In the parameterisation, however, the remaining ice is distributed evenly across the cloud and thus the sublimation process does not slow down and the cloud vanishes soon. In spite of these differences, all four models show identical humidities once all clouds have disappeared, meaning that the total amount of water is conserved in all models and none is lost in the cloud formation and dissipation process. These statements may change if cloud edge erosion or an ice mass threshold for the cloudiness of air parcels are included into the simulations. But the general result that allowing in-cloud subsaturation decelerates the sublimation process, and thereby increases cloud life time should remain valid.

The value of α strongly depends on the number density of ice crystals that is generated upon nucleation. If the number density is considered to be ten times larger than in the previous experiments, α grows to a value of $2.8 \cdot 10^{-3}$s^{-1}, which corresponds to a phase relaxation time of only 6 minutes (20). The resulting humidity evolutions of such an increase are shown in figs. 3.3 and 3.4, where the two new parameterisations are represented together by one plot in

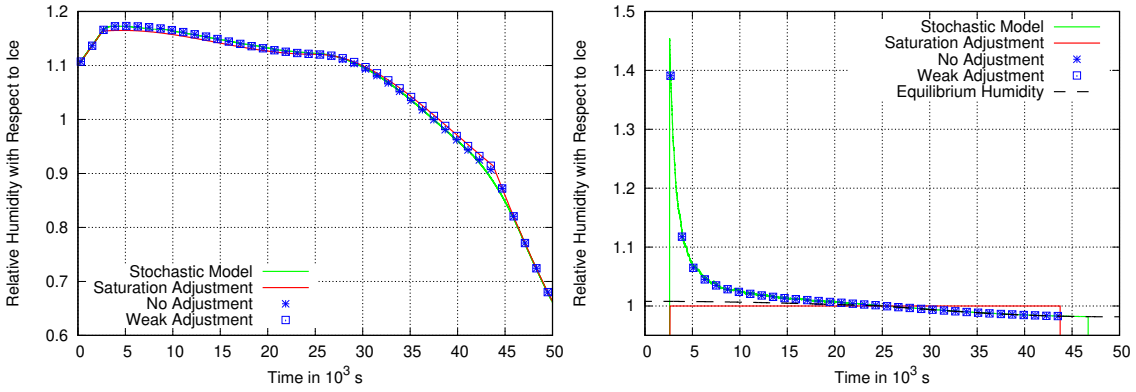

Figure 3.4: Scenario 2, but with $\alpha = 2.8 \cdot 10^{-3}$ s^{-1}, which corresponds to a cloud with 1000 crystals of 10 μm radius per litre.

fig. 3.3, since they provide identical results under cooling conditions as already noticed in the first experiment. Note that α has no effect on the saturation adjustment parameterisation, which means that the red curves are the same as in figs. 3.1 and 3.2.

Apparently, only small differences in the grid box mean humidity remain between the four models if the supersaturation is consumed by the ice crystals very fast. Especially, the adjustment performed in the weak adjustment parameterisation half way through the simulation is negligible, since the in-cloud humidity has already pretty much arrived at S_{eq} by this time any way (Fig. 3.4, right panel) so that the two new parameterisations almost do not differ at all. Furthermore, both reasons for the underestimation of supersaturation by saturation adjustment that were explained earlier become less important in this case. First, there still is considerable supersaturation inside the cloud shortly after the initiation of cloud formation, which is not at all represented by saturation adjustment (right panels). But it is consumed so quickly that it has already mostly been deposited as ice by the time the cloud fraction reaches values large enough that the in-cloud supersaturation could have a significant impact on the grid mean humidity. Secondly, S_{eq} is close to saturation if so many ice crystals are present, since any change in relative humidity due to temperature variations can quickly be compensated by deposition or sublimation if the available surface area is large. Thus, the initial supersaturation in newly generated cloud parts does not only decrease fast, it also decreases to almost saturated conditions, which makes saturation adjustment a fairly good approximation in such situations. Furthermore, also the cloud life times are more similar in this case, as the sublimation process in the other models becomes comparably rapid to saturation adjustment as well.

Gierens et al. (9) pointed out that the sub-grid variability in atmospheric properties decreases with rising spatial resolution such that the actual spread in specific humidity across a modern NWP grid box is probably often less than $\pm 25\%$. If a smaller sub-grid variability in humidity of only $\pm 10\%$ is assumed, the cloud fraction increases and decreases more rapidly. Figs. 3.5 and 3.6 show that this means, cloud formation is initiated later at a higher grid box mean relative humidity, since the top end of the humidity distribution is now lower and thus RH_{nuc} is reached later. Thereby higher grid box mean supersaturations are reached in all models.

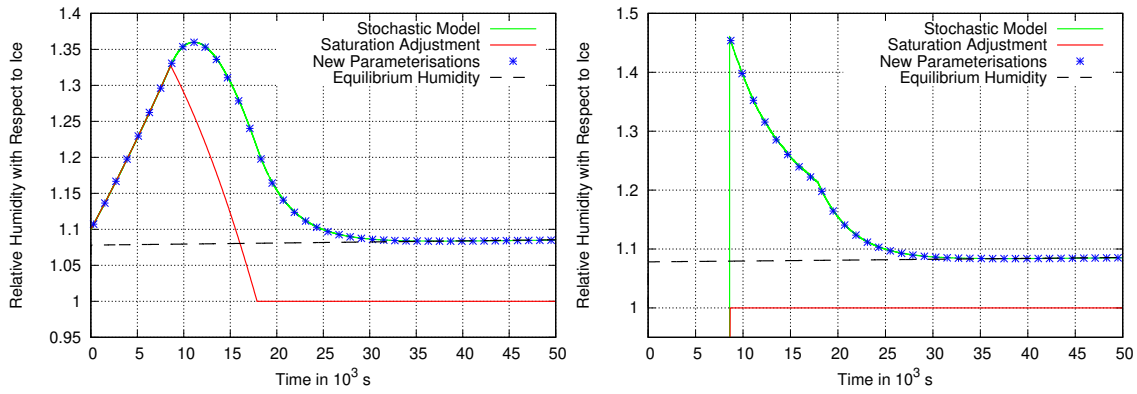

Figure 3.5: Scenario 1, but with a narrower initial humidity distribution ($a = 0.1$).

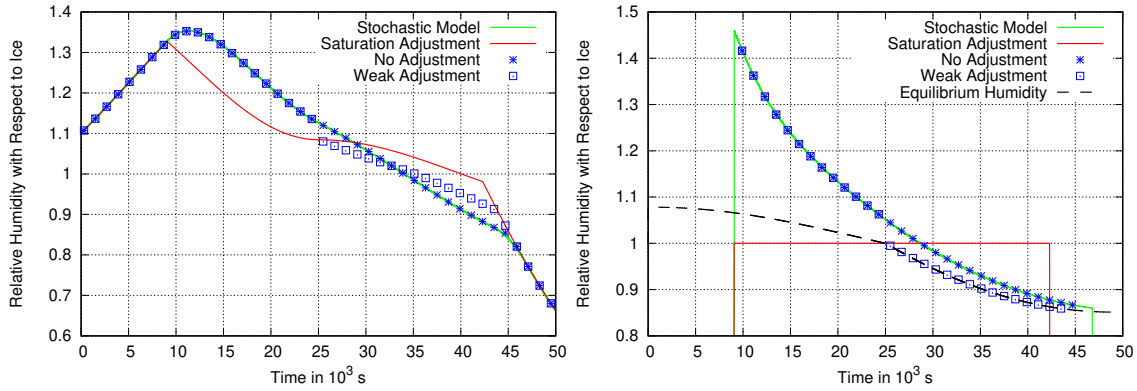

Figure 3.6: Scenario 2, but with a narrower initial humidity distribution ($a = 0.1$).

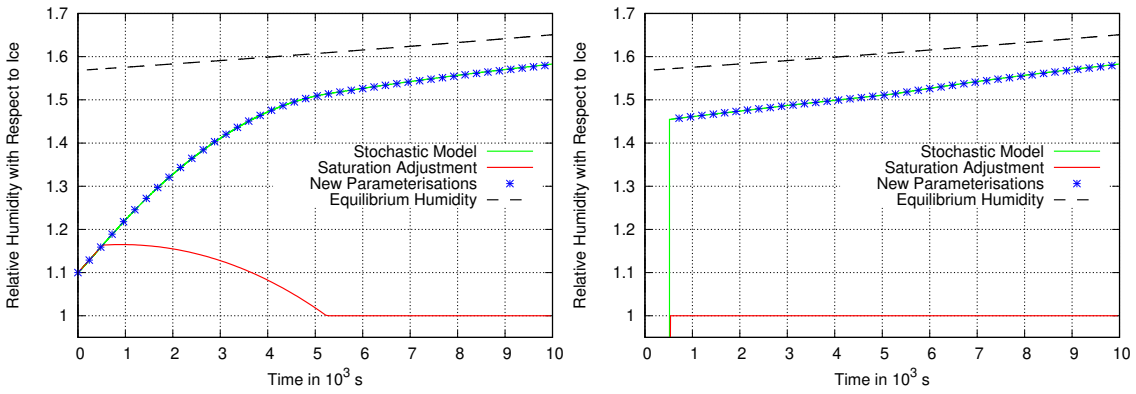

Figure 3.7: Scenario 1, but with a faster updraught of $w = 10\,\mathrm{cm\,s^{-1}}$. Note the different time scale.

Once cloud formation has commenced, the quickly growing cloud depletes the grid box mean supersaturation faster (left panels) and overcast conditions are reached earlier in all models (Fig. 3.5, right panel) despite the later begin of nucleation. When looking closely, one recognizes that the deviation of the saturation adjustment parameterisation from the stochastic model is even increased. This is, because the initially large difference in in-cloud humidity to the stochastic model gains significant weight in the grid mean humidity more quickly, if cloud fraction increases faster. Specifically, the maximum deviation in scenario 1 increases from less than 15 percentage points in figure 3.1 to about 20 percentage points in figure 3.5 and the maximum deviation in scenario 2 increases from less than 10 percentage points (fig. 3.2) to more than 10 points (fig. 3.6, always left panel). Accordingly, an even greater improvement can be expected from the new parameterisations the narrower the distribution of clear sky humidity is.

The equilibrium supersaturation rises quickly with increasing cooling rates. Figure 3.7 shows that it can even rise beyond the nucleation threshold in a rather extreme case of $10\,\mathrm{cm\,s^{-1}}$ constant updraught. This means, the air cools so quickly that q_s drops faster than the water molecules can deposit on the available ice surface. As a result, the difference between q and q_s grows more and more and thus the rise in relative humidity before nucleation is only slowed down by cloud formation and not reversed into a decay towards saturation as before. In such a case, the relative humidity provided by saturation adjustment is not only wrong but even shows a wrong trend. However, this simulation soon becomes unrealistic as the large supersaturation would make the ice crystals grow quickly in size and number. Hence, the available surface for vapour deposition would increase and with it the value of α. This then would make S_{eq} decrease and the humidity inside the cloud would follow it soon. Nevertheless, this simulation shows that extremely large supersaturations that are occasionally found in the upper troposphere can in principle be represented for short time intervals in the new parameterisations. To the contrary, supersaturations beyond the nucleation threshold are impossible in saturation adjustment.

A time step of one minute is still rather short in NWP. In order to test the stability of the new parameterisations against variations of the time step length, the two scenarios were also

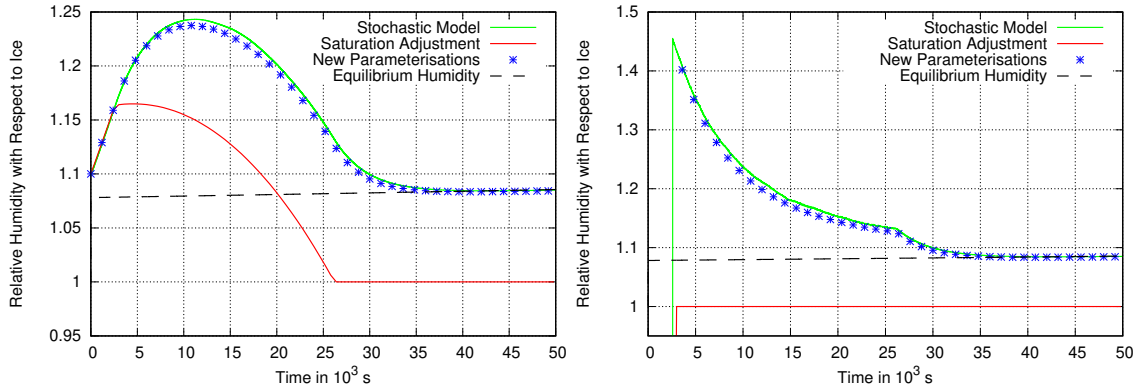

Figure 3.8: Scenario 1, but with a time step of 10 min.

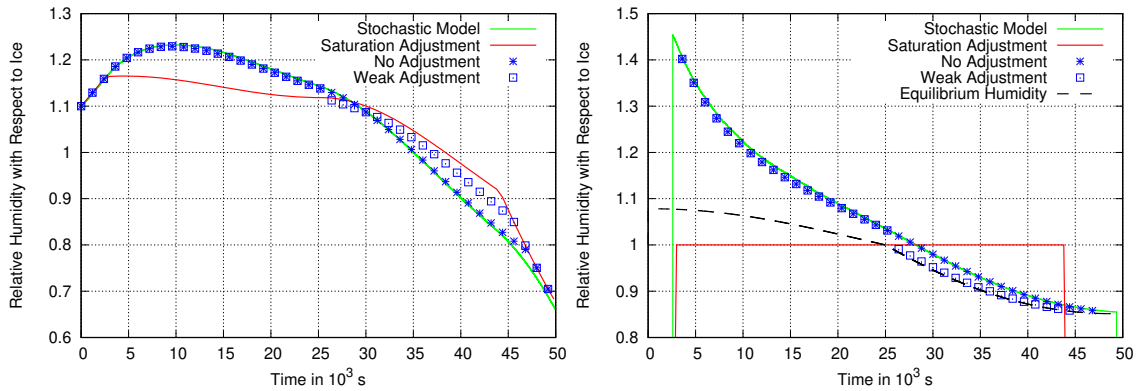

Figure 3.9: Scenario 2, but with a time step of 10 min.

repeated with a time step of ten minutes. Comparing the results of these experiments shown in figs. 3.8 and 3.9 with figs. 3.1 and 3.2 respectively, one can clearly see that the sensitivity is low. The new parameterisations still capture the onset of cloud formation precisely and also later on show a very similar behaviour as before. Also, the four models still show identical specific humidities at the end of scenario 2 (not shown) so that no water is added or lost during the simulation. The minor deviation in relative humidity at the very end in the left panel of fig. 3.9 is rather due to an error in temperature because of the rough approximation of the time dependence of the vertical wind. Finally, the time step was even increased to 30 minutes and the new parameterisations still showed a similar behaviour (not shown).

Overall, the new parameterisations always stayed closer to the stochastic box model than the adjustment parameterisation in all performed simulations and thus proved to be numerically stable against variations of the considered parameters and also likely are an improvement to the saturation adjustment method.

Chapter 4

Discussion

4.1 Determining the Deposition Rate

The first performed sensitivity study (Figs. 3.3 and 3.4) showed that the relative humidities provided by the new parameterisations become more similar to the ones calculated by using saturation adjustment if the value of the deposition rate α is large. With rising α, i.e. if more and larger ice crystals are present, the deposition of water vapour becomes more and more rapid due to the enlarged ice surface available to molecular exchange, resulting in a quicker decay of the initial supersaturation. Furthermore, the equilibrium supersaturation to which the humidity decays in the new parameterisations approaches zero for large values of α (cf. eq. 2.9) such that also the second reason for the underestimation of supersaturation under saturation adjustment vanishes in this limit. In fact, one could conceive saturation adjustment as a special case of the parameterisation without humidity adjustment, specifically one with an infinitely large α such that deposition and sublimation become instantaneous and thus any deviation from saturation inside the cloud is immediately balanced. In the weak adjustment parameterisation the analogy is a little more complicated. The value of α is the same as in the parameterisation without humidity adjustment in the calculation of S_{eq}. However, the decay towards S_{eq} becomes infinitely fast in the case of warming in partially cloudy skies. Therefore, the effective value of α describing the speed of deposition is infinite at the onset of warming, when the remaining supersaturation is actually adjusted to zero. Afterwards, the weak adjustment parameterisation shows even greater in-cloud subsaturation than the parameterisation without humidity adjustment (cf. fig. 3.2) meaning that the effective α returns to a similar but even smaller value.

Given these connections, the question arises, whether it is useful at all to replace saturation adjustment or whether the differences between these parameterisations in realistic situations are negligible anyway. The latter would be the case if the value of α was commonly large such that the decay of supersaturation inside cirrus clouds was typically fast compared to the time step length of a modern NWP model. α is the reciprocal value of the phase relaxation

time given by Khvorostyanov and Sassen (19) and can thus be estimated as

$$\alpha = 4\pi\, D\, N\, \overline{r}, \tag{4.1}$$

where D is the temperature and pressure dependent water vapour diffusion coefficient, N is the number density of ice crystals and $\overline{r}$ is their mean equivalent radius, i.e. the radius ice crystals with the same number density and the same total ice mass would have on average if they were spherical. In this equation, the diffusion coefficient exhibits the smallest variability under atmospheric conditions (36), while the number density and crystal radius vary over several orders of magnitude (6, 15, 23, 21, 22). In consequence, a large range of values can be considered realistic for α, but the data in these papers indicate that large values of N and $\overline{r}$, and thus large values of α, are typical for liquid-origin cirrus while in-situ formed cirrus is rather characterised by low number densities and small radii. The new parameterisations were mainly designed for stratiform clouds, i.e. in-situ formed cirrus, for which we consequently can expect smaller values of α and thus more considerable and longer lasting in-cloud supersaturations. In contrast, liquid-origin cirrus which is usually generated by the model's cumulus parameterisation, should feature large deposition rates and the benefit of modelling in-cloud supersaturation in this kind of ice clouds will be smaller than for in-situ cirrus.

N and $\overline{r}$ are available properties in a two-moment scheme, but unknown in one-moment parameterisations like the ones developed in this thesis. In principle, a solution could be estimating climatological mean values for α, possibly depending on climatological data at the respective geographical location, and applying them to all cirrus clouds in the new parameterisations. Unfortunately, such climatological data are not available for the upper troposphere. Also, once created, liquid-origin cirrus cannot be distinguished from in-situ formed cirrus in a one-moment scheme due to the lack of information about crystal number and size. The new parameterisations, despite being designed for in-situ formed cirrus, will therefore also have to process liquid-origin cirrus, once it is created by the cumulus parameterisation. A simple constant value of α would thus cause large errors in the in-cloud humidity in many cases, just as saturation adjustment, due to the mentioned large observed spread in N and $\overline{r}$. Determining α on the basis of the individual meteorological situation, i.e. estimating N and $\overline{r}$ from available model variables, hence appears inevitable.

Therefore, the question arises, what makes these properties in in-situ formed cirrus so different from liquid-origin cirrus. The difference responsible for the deviating number densities is the typical velocity of the updraught at the time of liquid or ice nucleation, respectively, where liquid-origin cirrus is usually formed in convective events commonly associated with strong updraughts, whereas in-situ formed cirrus is mostly generated in weak, synoptic scale updraughts. Considering that the atmospheric aerosol always features a size distribution, the smaller particles will require slightly larger supersaturations to nucleate a condensed, aqueous phase on them, whereas the larger ones will accumulate water earlier (Kelvin effect). Since nucleation occurs on a certain timescale, a stronger updraught can cause larger supersaturations beyond the respective nucleation threshold, before condensation or deposition become

effective and consume the supersaturation. Therefore, the stronger updraughts associated with liquid-origin cirrus may activate more aerosol particles leading to higher number densities of ice crystals. Notably, the water phase that is nucleating determines, how steep this increase of N with w is and it is less steep for the nucleation of liquid droplets (48). For homogeneous ice nucleation it was quantified by Kärcher and Lohmann (17) as

$$N \propto w^{3/2} \tag{4.2}$$

which could be used to estimate N in eq. 4.1. Importantly, they noted that the vertical velocity that has to be used in this equation is not the grid box mean velocity, as cirrus is most likely to form in the strongest updraughts inside a model grid box. Since compensating up- and downdraughts are common, they obtained an ice crystal number density 58-times larger than by using the grid box mean velocity when adding the average fluctuation to the mean vertical wind. These fluctuations in w can be estimated in the individual situation as $0.7\sqrt{\mathrm{TKE}}$, where TKE is the turbulent kinetic energy (26). In their model, Kärcher and Lohmann (17) obtain crystal number densities between $1l^{-1}$ and $1000l^{-1}$ for typical synoptic scale updraughts which is in good agreement with the values used in this thesis for the estimation of α ($100l^{-1}$, $1000l^{-1}$).

The difference between liquid-origin and in-situ formed cirrus responsible for the deviating mean equivalent radii is the origin of the respective air mass. Liquid-origin cirrus usually originates from lower tropospheric levels, where liquid droplets nucleate and rise up in convective events, before they freeze. These relatively warm air masses contain large amounts of water vapour in the beginning which successively condenses and later deposits onto the ice crystals on the way up forming crystals with large equivalent radii. The associated strong updraughts keep the crystals from falling, enabling their further growth. In contrast, in-situ formed cirrus arises from the dry, upper tropospheric air such that the available water vapour is commonly not sufficient for the generation of very large ice crystals. Additionally, large ice crystals cannot be carried by the associated weak, synoptic scale updraughts, causing them to sediment out quickly. The available water vapour thus sets a limit to the mean equivalent radius of the ice crystals. One could therefore approximate $\overline{r}$ by the radius spherical ice crystals with the number density estimated from w would have if the difference $q_{\mathrm{nuc}} - q_s$ between homogeneous nucleation threshold and saturation was deposited completely. This estimate might remind of saturation adjustment, but it is justified by the dependence $\overline{r} \propto \sqrt[3]{V}$, which means that a large fraction of the total growth of the crystals in radius already happens shortly after nucleation when their volume V is still small but grows most quickly. Using this approach, Kärcher and Lohmann (17) obtained crystal radii between about $5\mu m$ and $200\mu m$ for typical synoptic scale updraughts, which again means that the value of $10\mu m$ used to estimate α here is in a realistic range. Hence, the values of α used in this thesis can be considered the correct order of magnitude for in-situ formed cirrus and therefore significant differences in grid-mean supersaturation compared to saturation adjustment can indeed be expected when implementing the new parameterisations.

However, the amount of improvement from implementing the new concept will depend on the

temporal resolution of the respective model. If one uses the values of $\overline{r}$ and N from Kärcher and Lohmann (17) to obtain realistic values of the phase relaxation time from Khvorostyanov and Sassen (20), i.e. the e-folding time of supersaturation inside an air parcel, one obtains values for synoptic scale updraughts between about 12 minutes and 5 hours. Additionally, one should account for the fact that the in-cloud mean humidity relaxes slower than the supersaturation of a single parcel, since new highly supersaturated parcels keep joining the cloud as long as cooling proceeds (cf. fig. 3.1, right panel, the corresponding phase relaxation time is 1 hour here, e-folding takes about 3 hours). A high resolution NWP model with a time step of 5 minutes thus will show large in-cloud supersaturation shortly after the onset of nucleation in nearly all in-situ formed cirrus, while in a climate model with a time step of 30 minutes the in-cloud humidity may have relaxed quite far already one time step after nucleation in some cases. The benefit of the new concept then reduces to the difference between the equilibrium humidity and saturation. However, for liquid-origin cirrus the phase relaxation times may likely go down to the order of seconds such that a benefit from modelling the decay of in-cloud humidity may not be expected for this kind of ice clouds, since also the equilibrium supersaturation is negligible if deposition becomes that fast.

As has been shown, α can be recalculated every time step based on the current meteorological conditions. In some first tests of these ideas, α was varied with $w^{3/2}$ throughout the simulation (results not shown). If the same $\alpha[w(t)]$ was applied to all air parcels in the stochastic box model, the results of the new parameterisations were again very similar to the box model humidities. However, in fact, the number density of ice crystals in an air parcel would be determined by the updraught's velocity at the time of nucleation in this parcel. Thus, a different value of α would be valid for every air parcel. This is not possible to implement in the new parameterisations, as only one mean value of α is used in the calculations. Also, the updraught velocities at passed nucleation events, as well as the absolute supersaturations, are not kept in memory such that α can only be estimated from the current values of w and $q_{\mathrm{nuc}} - q_s$. Therefore, moderate differences to the box model results appeared in a simulation, where every air parcel in the box model deposited its water vapour at a speed depending on the updraught at its individual nucleation event. Obviously, this is a rather complicated situation which can no longer be fully captured in a one-moment scheme and further research is needed on how to determine α in the most suitable way.

As already mentioned, N and $\overline{r}$ are available parameters in two-moment ice schemes. Hence, α could be readily calculated in such parameterisations without further approximations. A complex two-moment scheme with detailed microphysics may not benefit from calculating in-cloud humidity according to the new concepts. However, such schemes are computationally expensive and it thus is not clear whether they can be used in NWP effectively. A combination of the new concept with a simplified two-moment scheme hence might be fruitful.

Further, complex influences on the distribution of supersaturation within cirrus clouds that would have to be accounted for in the calculation of α may arise from advection and sedimentation processes which have not been considered so far in the development of the new concept. Models implementing saturation adjustment do not face these influences, since here

α simply equals infinity and the in-cloud humidity distribution is a δ-distribution without any sensitivities to any other processes. An investigation of the behaviour of the new parameterisations in a more complete framework including advection and sedimentation is out of scope for the present thesis, but is of course the necessary next step on the way of implementing the new concept into an actual NWP model.

4.2 Further Applied Simplifications

Apart from the simplified vapour deposition using α (eq. 2.3), several other simplifications have been applied in this thesis. Some of these are straightforward to replace by more physical approaches and have only been implemented, since conceptual changes are not expected. Among these, there is the assumption of constant pressure which would be fairly easy to correct, but would likely have minor impact on the simulations since pressure only enters the calculations through the saturation specific humidity. Moreover, there is the negligence of radiative effects and latent heat which would state additional terms in the calculation of ΔT, where the former would usually be provided by the model's radiation scheme and the latter would be a feedback of the new parameterisations to temperature. In fact, however, the amount of latent heat typically realised by deposition and sublimation in the dry upper troposphere is generally negligible compared to the contributions to ΔT by radiation and vertical motion. Furthermore, clouds and radiation of course interact strongly, but in principle it is irrelevant to relative humidity by which means temperature changes are caused such that the negligence of radiative effects should not be of large importance to the general results.

Another feature, fairly easy to add, would be a threshold on q_i below which an amount of residual ice inside a grid box is not considered a cloud any more during the process of cloud dispersal. By setting such a threshold, the cloud fraction can be modelled more realistically, as optically very thin cirrus clouds become practically transparent and thus should no longer contribute to the cloud fraction. This is important for the radiation scheme in NWP as well as for contrail avoidance, since contrails in overcast skies do not need to be avoided, as the long-wave radiation from Earth's surface is absorbed by the natural cirrus anyway. The additional warming effect of the contrail then becomes negligible. This, however, is not the case if the cirrus is optically thin.

Other simplifications, such as the simplified deposition using α, have been more involved in the development of the new concept and thus cannot be corrected easily in the new parameterisations. One further example is the negligence of the temperature dependences of S_{nuc} and S_{eq} when deriving the evolution of an air parcel's supersaturation in time (eq. 2.10). This was necessary in order to retrieve an explicit expression for $S_p(t_1,\, t_{\mathrm{nuc}})$ analytically. However, since the subsequently derived in-cloud humidity distribution is always only applied for the current time step in the new parameterisations, this approximation is fairly good, as S_{nuc} and S_{eq} only vary weakly with temperature (cf. fig. 2.1). The same holds for the assumption of a uniform distribution of nucleation times t_{nuc} among the air parcels (eq. 2.11) in the derivation of the in-cloud humidity distribution. As fig. 2.2 shows, these assumptions did not severely

degrade the derived distribution, since it closely captures the simulated distribution in the stochastic box model.

Heterogeneous nucleation could be introduced into the new concept by setting another nucleation threshold typical for this kind of ice formation. Analogous to homogeneous nucleation, small amounts of water vapour would be transformed to ice, whenever an air parcel's supersaturation passes this new threshold. Furthermore, one could introduce a new cloud fraction C_{het} in order to keep track of how large the portion of the grid box is in which heterogeneously nucleated ice crystals deposit water vapour. Just as $C > 0$ is a trigger for deposition at the rate α in the present version of the parameterisations, $C_{\text{het}} > 0$ could then be the trigger for additional deposition at a new rate $\beta < \alpha$ typical for heterogeneous nucleation. However, the introduction of another nucleation pathway includes further complications such as the question of how to deal with the two cloud fractions; how they are added and how it can be assured that the overall cloud fraction does not exceed unity. Haag et al. (14) suggest based on in-situ measurements that even in the polluted regions of the northern hemisphere, where larger number concentrations of ice nuclei can be expected, cirrus clouds are not formed exclusively by heterogeneous nucleation. Thus, the impact of including this process into the new parameterisations can be expected to be minor anyway.

Another process neglected in the performed tests is cloud edge erosion which simulates the mixing of cloud air with the cloud free environment at the edge of a cloud inside a partially cloudy grid box. However, in the case of cirrus clouds in the new parameterisations, the cloud edge would not really "erode" in most cases, as the environmental air would be supersaturated as well. Hence, a mixing of ice germs into the environmental air would only cause further deposition and an expansion of the cloud. An inclusion of cloud edge erosion can thus be expected to lead to an even quicker increase in cloud fraction giving even more weight to the in-cloud supersaturation in the grid-mean humidity. An accelerated relaxation of the in-cloud supersaturation, however, may not be expected as the number of ice crystals is not increased. The result may therefore be an even more pronounced difference in grid-mean humidity between saturation adjustment and the new parameterisations shortly after nucleation. Only after longer periods of warming, when the cloud free environment has reached subsaturation, but the cloud still has not disappeared, mixing at the cloud edge would lead to a decrease in cloud ice and cloud fraction due to enhanced sublimation. Clouds may therefore actually disperse quicker than estimated by all models in this thesis possibly leading to in-cloud subsaturation being more rare. However, it also has been shown that allowing in-cloud subsaturation slows down the sublimation of cloud ice, as large amounts of ice have to be converted to vapour in saturation adjustment in order to keep the air inside the cloud saturated. Cloud lifetimes may therefore be underestimated in saturation adjustment and a replacement by one of the new parameterisations may lead to an improvement of this issue as well.

The clear sky humidity distribution was assumed to be uniform. This is quite a rough approximation given the observed distributions in Gierens et al. (9) which show a pronounced peak at the grid-box mean relative humidity decaying quickly into long distribution tails up

to ±100%. However, in this thesis, the uniform distribution, also used in the current version of the IFS, was assumed for easier comparability and also because it allowed an analytical derivation of the in-cloud humidity distribution (eq. 2.15) under certain assumptions. Nevertheless, the new concept is not bound to the uniform assumption. It might not be possible to derive the in-cloud humidity distribution analytically from a more complicated clear sky distribution, but it could still be fitted numerically to the output of the stochastic box model. Introducing a more realistic clear sky humidity distribution may thus be a way of improving the new parameterisations further. Moreover, Gierens et al. (9) showed that the width of this distribution decreases with increasing resolution. A modern NWP model grid box may thus likely feature less fluctuations in relative humidity than the ±25% assumed in the IFS. Figs. 3.5 and 3.6 show that a narrower clear sky humidity distribution does not only cause larger differences between saturation adjustment and the new parameterisations due to a more rapid increase in cloud fraction giving more weight to the initial large in-cloud supersaturation in the grid box average; it also leads to overall larger supersaturations in all models including the one using saturation adjustment. The reason is that the clear sky humidity distribution does not extent so far up from the mean value in such a case and thus hits the threshold for homogeneous nucleation later at a larger mean supersaturation. Accordingly, a simple improvement on the problem of systematic underestimation of upper tropospheric supersaturation in current NWP (10) without replacing the parameterisation itself might be assuming a narrower clear sky humidity distribution.

4.3 Comparison of the Parameterisations

Tompkins et al. (47) noted that many ice cloud schemes suffer from artificial sub-grid humidity fluxes between the cloudy and the clear sky parts of the grid boxes. These fluxes may occur if the specific humidities inside the cloud and in the cloud free environment are estimated via a diagnostic assumption. The most simple such assumption one could think of is that both, the in-cloud as well as the environmental humidity, equal the grid mean value (27). If water vapour is deposited inside the cloud, the in-cloud humidity should decrease, while the environmental humidity should remain unchanged. However, such a scheme would assume equal humidities again at the beginning of the next time step which corresponds to an artificial flux of humidity from the environment into the cloud. This is a rather simple example, but all parameterisations investigated by Tompkins et al. (47) suffered from these fluxes. Apparently, the system seems to lack information which is why one either has to apply such a diagnostic assumption or somehow recover the value of one of the sub-grid humidities from the previous time step. In saturation adjustment and the new parameterisation without humidity adjustment, the value of the in-cloud humidity at the end of the previous time step is simply known, either because it is exact saturation or because the value is memorized by the model, respectively.

In contrast, the weak adjustment parameterisation tries to deal with the information available in the system as long as possible and thereby has proven that the available information is

actually only insufficient if the grid box is warmed under partially cloudy conditions. In this case, information about the clear sky humidity distribution is lost, since it is no longer in contact with the nucleation threshold. Hence, in this situation, this parameterisation needs to set one of the two sub-grid humidities, in this case the in-cloud humidity, to a value as close as possible to the actual, unknown value, in this case the equilibrium humidity. This process is similar to saturation adjustment with the important difference that the value to which the in-cloud relative humidity is adjusted varies in between the time steps, since it depends on the current rate of temperature change. Despite being a more realistic value for the in-cloud humidity, this has the drawback that the final value from the previous time step generally does not equal the initial value of the next time step. Consequently, the weak adjustment parameterisation is not able to recover the exact in-cloud humidity from the previous time step if warming occurs in partially cloudy skies which makes the performed adjustment a form of diagnostic assumption. Accordingly, an artificial sub-grid humidity flux occurs, as the difference between the equilibrium humidity at the end of the previous time step and the one at the beginning of the next time step is added to the environmental humidity which is estimated on the basis of the in-cloud humidity. This flux is not inconsequential, since this humidity exchange with the clear sky part affects the sublimation rate. Fortunately, partially cloudy grid boxes become more and more rare in NWP, as the resolution of the models increases; grid boxes in high-resolution, regional models mostly are either completely covered or clear sky in which cases the two new parameterisations provide identical results. Hence, the higher the resolution of the model, the less often will the weak adjustment parameterisation differ from the parameterisation without humidity adjustment. Nevertheless, from a scientific point of view, the latter should be the preferred parameterisation as it does not only exhibit no artificial fluxes of humidity if partially cloudy grid boxes are warmed, but it also is more accurate in general in such cases.

However, another factor that has to be considered in evaluating the potential of the new parameterisations are the computational costs associated with their use. Calculating 850 time steps took about 7 ms in the current version of the parameterisation without humidity adjustment, while the weak adjustment parameterisation took about 6.5 ms for the same amount of steps on the same computer. For comparison, the adjustment parameterisation took only about 4.5 ms for this calculation. The difference between the two new parameterisations thus might not seem large, but an additional increase in run time has to be expected for the parameterisation without humidity adjustment since the new prognostic variable implemented in this scheme has to be processed by the core model. The weak adjustment parameterisation can thus be expected to be computationally cheaper, even though it is still associated with a significantly longer run time than saturation adjustment. Which of the two new parameterisations is the more suitable for a specific NWP model, therefore may depend on the resolution of the model, as the weak adjustment parameterisation might do sufficiently good in high-resolution models, where partially cloudy grid boxes that experience warming are rare. In such models, the weak adjustment parameterisation may produce comparably good results without the need for an additional prognostic variable. However, this hypothesis would need to be tested first.

In principle, one could think of several more possible parameterisations by combining different components of the ones presented here. The most simple one allowing in-cloud sub- and supersaturation would be adjusting the in-cloud humidity to the equilibrium humidity from eq. 2.9 instead of exact saturation as in the case of saturation adjustment. This way, one could achieve more realistic in-cloud humidities, at least for aged cirrus, where the supersaturation has already approached the equilibrium humidity quite far, at very little additional computational cost. However, this parameterisation would suffer from the mentioned artificial, sub-grid humidity fluxes all the time which makes it a rather unattractive alternative. A variation of the weak adjustment parameterisation avoiding these sub-grid fluxes would be reverting to saturation adjustment, whenever partially cloudy grid boxes experience warming. Thereby, the parameterisation would become a lot more simple in these cases and any unphysical sub-grid fluxes would vanish, while the benefits of the new concept would remain in all other situations. The obvious drawback would be the negligence of in-cloud subsaturation in partially cloudy grid boxes. This, however, might not cause a too large error in the overall humidity statistics generated by such a parameterisation due to the mentioned decreasing occurrence frequency of partially cloudy grid boxes in modern NWP.

In the end, a temporally and spatially precise forecast of ice supersaturation will not be achieved without the aid of upper tropospheric humidity measurements for data assimilation, as argued in the introduction, no matter which parameterisation is used in which model. The new concept alone may only make a model's humidity statistics better match the corresponding statistics obtained from the measurements taken over many years in the MOZAIC (Measurement of ozone and water vapor by Airbus in-service aircraft, 28) and IAGOS projects (In-service Aircraft for a Global Observing System, 35). But this is only a necessary, not a sufficient condition for a more reliable forecast on a specific day. More commercial aircraft equipped with hygrometers that work reliably in the upper troposphere are urgently needed.

Chapter 5

Summary and Conclusions

In this thesis, the concept for a new one-moment ice cloud scheme avoiding the practice of saturation adjustment common in numerical weather prediction (NWP) has been proposed. Parameterisations applying saturation adjustment allow supersaturation with respect to ice in clear air, but adjust humidity to exact saturation inside ice clouds even though supersaturated air is frequently observed inside cirrus. Accordingly, such models have been shown to underestimate the occurrence frequency and degree of ice supersaturation in the upper troposphere. Since this supersaturation is an important condition for the persistence of contrails which is responsible for a large fraction of aviation's overall effective radiative forcing, this inaccuracy of NWP turns out to be a problem for eco-efficient flight routing.

In order to address this issue, a stochastic box model that simulates a large number of air parcels representing one grid box of a NWP model has been developed in this thesis. Each air parcel is given an individual specific humidity thereby representing sub-grid scale fluctuations in the humidity field. If nucleation occurs inside an air parcel, the reduction in specific humidity associated with the deposition of water vapour is approximated to be an exponential decay towards saturation. In this model, lifecycles of ice clouds have been simulated and the humidity distributions inside them have been studied. When comparing the evolution of the mean humidity across all air parcels to a parameterisation using saturation adjustment, it was revealed that the underestimation of supersaturation due to saturation adjustment is twofold:

1. Shortly after the onset of cloud formation, the cloud in the stochastic box model is still highly supersaturated, as the water vapour is only successively deposited onto the ice crystals. Saturation adjustment transforms all supersaturation to ice within one time step and leaves the cloud at exact saturation.

2. If the grid box experiences continuous cooling, supersaturation keeps getting restored in the stochastic box model such that an equilibrium supersaturation of a few percent remains inside the cloud, even long after nucleation. With saturation adjustment, there is no in-cloud supersaturation at all.

Furthermore, saturation adjustment may also lead to an overestimation of humidity whenever

warming occurs inside a cloud. In this case, the ice crystals do not sublimate instantaneously in the stochastic box model such that an equilibrium subsaturation is approached, where the reduction in relative humidity due to warming equals the increase due to sublimation. In contrast, saturation adjustment again simply assumes saturated conditions inside the cloud.

The new concept for an improved treatment of humidity inside ice clouds is based on an analytical expression for the mean of the humidity distribution in newly generated cloud parts in the stochastic box model. Unfortunately, the system of common NWP model variables does not seem to incorporate sufficient information to divide a grid box into the cloudy and the clear sky part under all circumstances; specifically it seems to lack information under warming conditions in partly cloudy skies. Two alternative parameterisations solving this problem in different ways have been presented. The first one, referred to as "weak adjustment parameterisation", assumes that the in-cloud humidity will have approached its equilibrium value sufficiently close by the time cooling reverses into warming inside the cloud. Thus, it adjusts the in-cloud humidity to the equilibrium value, whenever partly cloudy grid boxes experience warming, hence reverting to some kind of humidity adjustment similar to saturation adjustment. This parameterisation therefore suffers from reduced accuracy and also from artificial sub-grid humidity fluxes between the cloud and its environment in these situations. The second parameterisation adds new information to the system by introducing the in-cloud humidity as a new prognostic variable. Thereby, its accuracy remains on the same, high level in all situations considered here and also artificial sub-grid fluxes of humidity are avoided. However, the new prognostic variable will be associated with increased computational costs, as it has to be processed by the core model.

In all performed simulations, the new parameterisations provided more accurate results than saturation adjustment, where the mean humidity across all air parcels in the stochastic box model served as a benchmark to which the parameterisations were compared. The parameterisation without humidity adjustment closely followed the stochastic box model in different updraught scenarios with different rates of exponential humidity decay, different widths of the clear sky sub-grid humidity distribution and different time step lengths. The weak adjustment parameterisation provided identical results with the exception of warming in partially cloudy skies where it was less accurate, but still stayed closer to the stochastic box model than saturation adjustment.

The improvement associated with the new concept compared to saturation adjustment depends on how fast the in-cloud supersaturation decays after the onset of cloud formation in comparison with the length of the model time step. Therefore the benefit will probably be larger the higher the model's time resolution is, as clouds are more likely to be significantly supersaturated over multiple time steps in this case. In contrast, the improvement in the simulations was less if the rate of exponential humidity decay was assumed large, since the initial supersaturation decays quickly in such situations and also the equilibrium supersaturation to which it decays is small. Hence, both reasons for the underestimation of supersaturation due to saturation adjustment become less important. Such large deposition rates can be generated in strong updraughts which are uncommon for in-situ formed cirrus. Therefore,

deposition is generally slow compared to usual NWP model time steps in this kind of ice clouds and a significant improvement compared to saturation adjustment can be expected. In contrast, large deposition rates are typical for liquid-origin cirrus such that the benefit from implementing the new concept can be expected to be smaller in this kind of cirrus.

Furthermore, the improvement compared to saturation adjustment was enhanced, when cloud fraction increased quickly, as this gives more weight to the initially large in-cloud supersaturation in the grid box mean humidity. Fast increases in cloud fraction occur for example if the sub-grid humidity fluctuations in the clear sky are small. The benefit from implementing the new concept will therefore also likely be larger if the spatial resolution of the model is high, as this lowers the fluctuations in humidity inside the single grid boxes. Additionally, this should improve the accuracy of the weak adjustment parameterisation, since partially cloudy grid boxes that may experience warming are less frequent in high resolution.

The rate of exponential humidity decay mainly depends on the number density and the size of the ice crystals inside the cloud and thus varies in time. Even though this rate was assumed to be constant throughout all presented tests of the parameterisations, first simulations with a variable decay rate have provided promising results. Of course, further tests, especially in a less artificial environment, are needed, before these parameterisations can actually contribute to an improvement in the forecasts of ice supersaturation on cruise levels and therefore to an improvement in contrail avoidance.

Note on Similarity

The research described in this thesis is largely identical to what is discussed in Sperber and Gierens (43). Therefore, considerable parts of these publications are similar to equal. This is in agreement with Klaus Gierens.

Acknowledgements

I wish to thank all persons that supported me during the research and the writing of this thesis, especially

- Klaus Gierens for supervising me, introducing me into the field, suggesting suitable literature, answering any scientific questions and giving helpful suggestions, whenever I needed them. It was great fun working with you and I always felt in good hands.
- Robert Sausen for introducing the topic to me and making contact to Klaus Gierens.
- Sabine Brinkop for helpful comments and suggestions.
- Sina Hofer, Moritz Witt, Ismail Makroum, Patrick Peter and Anna Götz for a welcoming and friendly atmosphere in our office.
- Anja Blum and Sina Hofer for a lot of help in organisational issues.
- Anja Schmidt for reviewing the thesis.
- my girlfriend Sophia Geisenhofer for motivating and encouraging me.

Without all of these people and many more this thesis would not have been possible.

Bibliography

[1] Appleman, H. (1953). The formation of exhaust condensation trails by jet aircraft. *Bull. Amer. Met. Soc.*, 34:14–20.

[2] Corti, T. and Peter, T. (2009). A simple model for cloud radiative forcing. *Atmos. Chem. Phys.*, 9:5751—-5758.

[3] Dekoutsidis, G., Groß, S., Wirth, M., Krämer, M., and Rolf, C. (2022). Characteristics of supersaturation in mid-latitude cirrus clouds and their adjacent cloud-free air. *Atmos. Chem. Phys. Disc.*, accepted Preprint:1–23.

[4] di ser Piero da Vinci, L. (1505). *Codice sul volo degli uccelli*.

[5] Dietmüller, S., Matthes, S., Dahlmann, K., Yama-shita, H., Simorgh, A., Soler, M., Linke, F., Lührs, B., Meuser, M., Weder, C., Grewe, V., Yin, F., and Castino, F. (2022). A python library for computing individual and merged non-CO2 algorithmic climate change functions: CLIMaCCF V1.0. *Geosci. Model Dev. Disc.*, under review.

[6] Dowling, D. and Radke, L. (1990). A summary of the physical properties of cirrus clouds. *J. Appl. Meteorol.*, 29:970–978.

[7] ECMWF (2021). *IFS Documentation CY47R3*. ECMWF.

[8] Gierens, K. (2003). On the transition between heterogeneous and homogeneous freezing. *Atmos. Chem. Phys.*, 3:437–446.

[9] Gierens, K., Kohlhepp, R., Dotzek, N., and Smit, H. (2007). Instantaneous fluctuations of temperature and moisture in the upper troposphere and tropopause region. part 1: Probability densities and their variability. *Meteorol. Z.*, 16:221–231.

[10] Gierens, K., Matthes, S., and Rohs, S. (2020). How well can persistent contrails be predicted? *Aerospace*, 7:169.

[11] Gierens, K., Schumann, U., Helten, M., Smit, H., and Marenco, A. (1999). A distribution law for relative humidity in the upper troposphere and lower stratosphere derived from three years of MOZAIC measurements. *Ann. Geophys.*, 17:1218–1226.

[12] Gierens, K., Spichtinger, P., and Schumann, U. (2012). Ice supersaturation. In Schumann, U., editor, *Atmospheric Physics. Background — Methods — Trends*, chapter 9, pages 135–150. Springer, Heidelberg, Germany.

[13] Gierens, K. and Vázquez-Navarro, M. (2018). Statistical analysis of contrail lifetimes from a satellite perspective. *Meteorol. Z.*, 27:183–193.

[14] Haag, W., Kärcher, B., Ström, J., Minikin, A., Lohmann, U., Ovarlez, J., and Stohl, A. (2003). Freezing thresholds and cirrus cloud formation mechanisms inferred from in situ measurements of relative humidity. *Atmos. Chem. Phys.*, 3:1791–1806.

[15] Heymsfield, A., Krämer, M., Luebke, A., Brown, P., Cziczo, D., Franklin, C., Lawson, P., Lohmann, U., McFarquhar, G., Ulanowski, Z., and Tricht, K. V. (2017). Cirrus clouds. *Meteorological Monographs*, 58:1–26.

[16] Kärcher, B. (2018). Formation and radiative forcing of contrail cirrus. *Nat Commun*, 9.

[17] Kärcher, B. and Lohmann, U. (2002). A parameterization of cirrus cloud formation: Homogeneous freezing of supercooled aerosols. *J. Geophys. Res.*, 107:doi: 10.1029/2001JD000470.

[18] Kaufmann, S., Voigt, C., Heller, R., Jurkat-Witschas, T., Krm̃er, M., Rolf, C., Zöger, M., Giez, A., Buchholz, B., Ebert, V., Thornberry, T., and Schumann, U. (2018). Intercomparison of midlatitude tropospheric and lower-stratospheric water vapor measurements and comparison to ecmwf humidity data. *Atmos. Chem. Phys.*, 18:16729—-16745.

[19] Khvorostyanov, V. and Sassen, K. (1998a). Cirrus cloud simulation using explicit microphysics and radiation. part i: Model description. *J. Atmos. Sci.*, 55:1808–1821.

[20] Khvorostyanov, V. and Sassen, K. (1998b). Cirrus cloud simulation using explicit microphysics and radiation. part ii: Microphysics, vapor and ice mass budgets, and optical and radiative properties. *J. Atmos. Sci.*, 55:1822–1845.

[21] Krämer, M., Rolf, C., Luebke, A., Afchine, A., Spelten, N., Costa, A., Meyer, J., Zöger, M., Smith, J., Herman, R., Buchholz, B., Ebert, V., Baumgardner, D., Borrmann, S., Klingebiel, M., and Avallone, L. (2016). A microphysics guide to cirrus clouds part 1: Cirrus types. *Atmos. Chem. Phys.*, 16:3463–3483.

[22] Krämer, M., Rolf, C., Spelten, N., Afchine, A., Fahey, D., Jensen, E., Khaykin, S., Kuhn, T., Lawson, P., Lykov, A., Pan, L., Riese, M., Rollins, A., Stroh, F., Thornberry, T., Wolf, V., Woods, S., Spichtinger, P., Quaas, J., and Sourdeval, O. (2020). A microphysics guide to cirrus – part 2: Climatologies of clouds and humidity from observations. *Atmos. Chem. Phys.*, 20:12569—-12608.

[23] Krämer, M., Schiller, C., Afchine, A., Bauer, R., Gensch, I., Mangold, A., Schlicht, S., Spelten, N., Sitnikov, N., Borrmann, S., de Reus, M., and Spichtinger, P. (2009). Ice supersaturations and cirrus cloud crystal numbers. *Atmos. Chem. Phys.*, 9:3505–3522.

[24] Lamb, D. and Verlinde, J. (2011). *Physics and Chemistry of Clouds*. Cambridge University Press.

[25] Lee, D., Fahey, D., Skowron, A., Allen, M., Burkhardt, U., Chen, Q., Doherty, S., Freeman, S., Forster, P., Fuglestvedt, J., Gettelman, A., De León, R., Lim, L., Lund, M., Millar, R., Owen, B., Penner, J., Pitari, G., Prather, M., Sausen, R., and Wilcox, L. (2021). The contribution of global aviation to anthropogenic climate forcing for 2000 to 2018. *Atmos. Env.*, 244:117834.

[26] Lohmann, U., Feichter, J., Chuang, C., and Penner, J. (1999). Predicting the number of cloud droplets in the ECHAM GCM. *J. Geophys. Res.*, 104:9169–9198.

[27] Lohmann, U. and Kärcher, B. (2002). First interactive simulations of cirrus cloud formed by homogeneous freezing in the echam general circulation model. *J. Geophys. Res.*, 107.

[28] Marenco, A., Thouret, V., Nedelec, P., Smit, H., Helten, M., Kley, D., Karcher, F., Simon, P., Law, K., Pyle, J., Poschmann, G., Wrede, R. V., Hume, C., and Cook, T. (1998). Measurement of ozone and water vapor by airbus in-service aircraft: The MOZAIC airborne program, an overview. *J. Geophys. Res.*, 103:25631–25642.

[29] McDonald, J. (1963). The saturation adjustment in numerical modelling of fog. *J. Atmos. Sci.*, 20:476–478.

[30] Meerkötter, R., Schumann, U., Doelling, D., Minnis, P., Nakajima, T., and Tsushima, Y. (1999). Radiative forcing by contrails. *Ann. Geophys.*, 17:1080–1094.

[31] Murphy, D. and Koop, T. (2005). Review of the vapour pressures of ice and supercooled water for atmospheric applications. *Quart. J. Roy. Met. Soc.*, 131:1539–1565.

[32] Ovarlez, J., Gayet, J.-F., Gierens, K., Ström, J., Ovarlez, H., Auriol, F., Busen, R., and Schumann, U. (2002). Water vapour measurements inside cirrus clouds in northern and southern hemispheres during INCA. *Geophys. Res. Lett.*, 29:1813, doi:10.1029/2001GL014440.

[33] Ovidius Naso, P. (8). *Metamorphoses VIII.*

[34] Petzold, A., Neis, P., Rütimann, M., Rohs, S., Berkes, F., Smit, H., Krämer, M., Spelten, N., Spichtinger, P., Nedelec, P., and Wahner, A. (2020). Ice-supersaturated air masses in the northern mid-latitudes from regular in situ observations by passenger aircraft: vertical distribution, seasonality and tropospheric fingerprint. *Atmos. Chem. Phys.*, 20:8157–8179.

[35] Petzold, A., Thouret, V., Gerbig, C., Zahn, A., Brenninkmeijer, C., Gallagher, M., Hermann, M., Pontaud, M., Ziereis, H., Boulanger, D., Marshall, J., Nedelec, P., Smit, H., Friess, U., Flaud, J.-M., Wahner, A., Cammas, J.-P., and Volz-Thomas, A. (2015). Global-scale atmosphere monitoring by in-service aircraft - current achievements and future prospects of the european research infrastructure iagos. *Tellus B*, 67.

[36] Pruppacher, H. and Klett, J. (1997). *Microphysics of clouds and precipitation.* Kluwer Academic Publishers, 2nd edition.

[37] Sausen, R., Hofer, S., Gierens, K., Bugliaro, L., Ehrmanntraut, R., Sitova, I., Walczak, K., Burridge-Diesing, A., Bowman, M., and Miller, N. (2023). Can we successfully avoid persistent contrails by small altitude adjustments of flights in the real world? *Meteorol. Z.*

[38] Schmidt, E. (1941). Die Entstehung von Eisnebel aus den Auspuffgasen von Flugmotoren. *Schriften der deutschen Akademie der Luftfahrtforschung*, 44:1–15.

[39] Schumann, U. (1996). On conditions for contrail formation from aircraft exhausts. *Meteorol. Z.*, 5:4–23.

[40] Schumann, U. (2012). A contrail cirrus prediction model. *Geoscientific Model Development*, 5:543–580.

[41] Schumann, U., Mayer, B., Graf, K., and Mannstein, H. (2012). A parametric radiative forcing model for contrail cirrus. *J. Appl. Meteorol. Climatol.*, 51:1391–1406.

[42] Shparberg, S. and Lange, B. (2022). Global market forecast 2022. Technical report, Airbus.

[43] Sperber, D. and Gierens, K. (2023). Towards a more reliable forecast of ice supersaturation: Concept of a one-moment ice cloud scheme that avoids saturation adjustment. *EGUsphere*, [preprint].

[44] Spichtinger, P., Gierens, K., Smit, H., Ovarlez, J., and Gayet, J.-F. (2004). On the distribution of relative humidity in cirrus clouds. *Atmos. Chem. Phys.*, 4:639–647.

[45] Teoh, R., Schumann, U., Gryspeerdt, E., Shapiro, M., Molloy, J., Koudis, G., Voigt, C., and Stettler, M. (2022). Aviation contrail climate effects in the north atlantic from 2016 to 2021. *Atmos. Chem. Phys.*, 22:10919—-10935.

[46] Teoh, R., Schumann, U., Majumdar, A., and Stettler, M. (2020). Mitigating the climate forcing of aircraft contrails by small-scale diversions and technology adoption. *Environ. Sci. Technol.*, 54:2941–2950.

[47] Tompkins, A., Gierens, K., and Rädel, G. (2007). Ice supersaturation in the ECMWF integrated forecast system. *Quart. J. Roy. Met. Soc.*, 133:53–63.

[48] Twomey, S. (1977). *Atmospheric Aerosols.*

[49] Wegener, A. (1914). Meteorologische Terminbeobachtungen am Danmarks-Havn. In *Meddelelser om Grønland, Vol. XLII: Danmark-Ekspeditionen til Grønlands Nordøstkyst 1906–1908, Vol. II*, pages 125–356. Kommissionen for ledelsen af de geologiske og geografiske undersøgelser i Grønland.

[50] Wilhelm, L., Gierens, K., and Rohs, S. (2021). Weather variability induced uncertainty of contrail radiative forcing. *Aerospace*, 8(332).

[51] Wilson, D. and Ballard, S. (1999). A microphysically based precipitation scheme for the UK meteorological office unified model. *Quart. J. Roy. Met. Soc.*, 125:1607–1636.

[52] Wolf, K., Bellouin, N., and Boucher, O. (2023). Radiative effect by cirrus cloud and contrails – a comprehensive sensitivity study. *EGUsphere*, Preprint:1–38.

[53] Yin, F., Grewe, V., Castino, F., Rao, P., Matthes, S., Dahlmann, K., Dietmüller, S., Frömming, C., Yamashita, H., Peter, P., Klingaman, E., Shine, K., Lührs, B., and Linke, F. (2022). Predicting the climate impact of aviation for en-route emissions: The algorithmic climate change function submodel ACCF 1.0 of EMAC 2.53. *Geosci. Model. Dev. Discuss.*, Preprint:gmd–2022–220.

Selbstständigkeitserklärung

Ich versichere hiermit, die vorliegende Arbeit mit dem Titel

Konzept eines Ein-Momenten Eiswolken Schemas ohne Sättigungskorrektur

selbstständig verfasst zu haben und keine anderen als die angegebenen Quellen und Hilfsmittel verwendet zu haben.

Dario Sperber

Reichertshausen, den 21. Juli 2023